Published in final edited form as:
*Nat Cancer*. 2021 July ; 2(7): 693–708. doi:10.1038/s43018-021-00221-9.

# Acquired resistance to anti-MAPK targeted therapy confers an immune-evasive tumour microenvironment and cross-resistance to immunotherapy in melanoma

**Lisa Haas**[1], **Anais Elewaut**[1], **Camille L. Gerard**[2], **Christian Umkehrer**[1], **Lukas Leiendecker**[1], **Malin Pedersen**[3], **Izabela Krecioch**[1], **David Hoffmann**[4], **Maria Novatchkova**[1], **Mario Kuttke**[1,§], **Tobias Neumann**[1], **Ines Pires de Silva**[5,6,7], **Harriet Witthock**[3], **Michel A. Cuendet**[2,8,9], **Sebastian Carotta**[10], **Kevin J. Harrington**[3], **Johannes Zuber**[1], **Richard A. Scolyer**[5,6,7,11], **Georgina V. Long**[5,6,7,12,13], **James S. Wilmott**[5,6,7], **Olivier Michielin**[2,8], **Sakari Vanharanta**[14], **Thomas Wiesner**[15], **Anna C. Obenauf**[1,*]

[1]Research Institute of Molecular Pathology (IMP), Vienna Biocenter (VBC), Vienna, Austria

[2]Department of Oncology, Lausanne University Hospital, Lausanne, Switzerland

[3]Institute of Cancer Research, 237 Fulham Road, SW3 6JB London, United Kingdom

[4]Institute of Molecular Biotechnology (IMBA), Vienna Biocenter (VBC), Vienna, Austria

[5]Melanoma Institute Australia, The University of Sydney, Sydney, Australia

[6]Charles Perkins Centre, The University of Sydney, Sydney, Australia



[*]Correspondence and request for materials should be addressed to Anna Obenauf: anna.obenauf@imp.ac.at.
[§]Current address: Institute of Vascular Biology and Thrombosis Research, Medical University of Vienna, Vienna, Austria.

**Author Contributions**

L.H. and A.C.O. conceived the study, designed the experiments, and interpreted the results. A.C.O. supervised the study. L.H. developed experimental tools, performed *in vitro* experiments, *in vivo* treatment studies, flow cytometry analysis, gene expression profiling, parts of the computational analysis and analysed the data. A.E. validated *in vivo* treatment studies in independent experiments, performed the *in vitro* co-culture in Fig. 3i, Fig. 4f and Fig. 7f and performed the ATAC-seq library prep. C.U. performed large parts of the SLAM-seq experiment (Extended Data Fig. 9d-h) and generated matched CaTCH clones (Fig. 5f, Extended Data Fig. 8e). I.K. performed immunoblotting and immune-fluorescence staining (including quantifications) and helped with mouse colony maintenance. M.P. and H.W. performed experiments involving focal radiation. M.K. helped with flow cytometry studies and *in vivo* studies (including CT26 flow cytometry characterization displayed in Extended Data Fig. 6k, m). D.H. contributed to experimental design, computational analysis, *in vivo* studies and data interpretation. C.L.G collected the patient information for the retrospective analysis in Fig. 1a, b. C.L.G, M.A.C. and O.V. analysed and interpreted the collected patient data. I.S. and G.V.L. provided updated survival information for the Gide et.al. dataset. J.S.W., G.V.L. and R.A.S. analysed and interpreted VECTRA image analysis data of melanoma biopsies and related clinical data of patients treated with MAPKi therapies and provided matched patient biopsies for the CLEC9a staining for Fig. 3g. L.L., M.N. and T.N. analysed gene-expression data, SLAM-seq data and WES data. L.L. analysed ATAC-seq data and contributed to experimental design and data interpretation. J.Z. provided conceptual input for experiment design and data interpretation of SLAM-seq. S.V. analysed RNA-seq data, generated the ccIES and probed it in RNA-seq data of TCGA and published melanoma patient datasets. S.C. and K.J.H provided conceptual input to experiment design and data interpretation. T.W. provided clinical expertise and input to experiment design, interpretation, and presentation. L.H., T.W. and A.C.O wrote the manuscript and all authors read and approved the manuscript.

**Conflict of Interests**

R.A.S has received fees for professional services from Qbiotics Group Limited, Novartis Pharma AG, MSD Sharp & Dohme (Australia), NeraCare, AMGEN Inc., Bristol-Myers Squibb, Novartis Pharmaceuticals Australia Pty Limited, Myriad Genetics GmbH, GlaxoSmithKline Australia. G.V.L. receives consultant service fees from Aduro, Amgen, Bristol-Myers Squibb, Mass-Array, Merck, MSD, Novartis, OncoSec Medical, Pierre Fabre, Roche, QBiotics and Sandoz. S.C. is an employee of Boehringer Ingelheim GmbH. J.Z. is a founder, shareholder and scientific advisor of Quantro Therapeutics GmbH. J.Z., A.O. and the Obenauf and Zuber labs receive research support and funding from Boehringer Ingelheim. The other authors declare no conflict of interest.


Europe PMC Funders Author Manuscripts

[7]Sydney Medical School, The University of Sydney, Sydney, Australia

[8]Molecular Modeling Group, Swiss Institute of Bioinformatics, UNIL Sorge, Lausanne, Switzerland

[9]Department of Physiology and Biophysics, Weill Cornell Medicine, New York, USA

[10]Boehringer Ingelheim RCV GmBH & Co KG, Vienna, Austria

[11]Royal Prince Alfred Hospital, & New South Wales Health Pathology, Sydney, Australia

[12]Royal North Shore Hospital, Sydney, Australia

[13]Mater Hospital, North Sydney, Australia

[14]MRC Cancer Unit, University of Cambridge, Cambridge, United Kingdom

[15]Department of Dermatology, Medical University of Vienna, Vienna, Austria



Europe PMC Funders Author Manuscripts

## Abstract

How targeted therapies and immunotherapies shape tumours and thereby influence subsequent therapeutic responses is poorly understood. Here, we show in melanoma patients and mouse models that when tumours relapse following targeted therapy with MAPK pathway inhibitors, they are cross-resistant to immunotherapies, despite the different modes of action of these therapies. We find that cross-resistance is mediated by a cancer cell-instructed, immunosuppressive tumour microenvironment that lacks functional $CD103^+$ dendritic cells, precluding an effective T cell response. Restoring the numbers and functionality of $CD103^+$ dendritic cells can re-sensitize cross-resistant tumours to immunotherapy. Cross-resistance does not arise from selective pressure of an immune response during evolution of resistance, but from the MAPK pathway, which is not only reactivated, but also exhibits an increased transcriptional output that drives immune evasion. Our work provides mechanistic evidence for cross-resistance between two unrelated therapies, and a scientific rationale for treating patients with immunotherapy before they acquire resistance to targeted therapy.

## Introduction

Targeted therapies, inhibiting oncogenic signalling in cancer cells, and immunotherapies, stimulating the immune system to eliminate cancer cells, have revolutionized the treatment of metastatic cancer patients and lead to durable tumour control in a subset of patients[1]. However, low response rates and acquired resistance remain daunting problems. Based on the different modes of action of targeted and immunotherapies and the expectation that resistance mechanisms are not overlapping, targeted and immunotherapies are often administered sequentially[2]. Yet how these therapies change the tumour and its microenvironment and thereby influence subsequent therapeutic responses remains poorly understood.

*BRAF*-mutated, metastatic melanoma exemplifies the sequential treatment approach, as it responds well to both classes of therapies. Targeted therapy with MAPK pathway inhibitors (RAFi, MEKi) leads to prompt responses in the majority of patients, however responses are often not durable with a median duration of response of approximately one year[3]. In

contrast, immunotherapy with checkpoint blockade antibodies directed against programmed cell-death protein 1 (PD-1) and cytotoxic T-lymphocyte-associated antigen (CTLA-4) results in durable responses in a subset of melanoma patients but shows lower response rates[4]. Therefore, the *ASCO* and *ESMO* guidelines recommend both targeted and immunotherapies as first-line treatment for metastatic melanoma[5,6]. However, there is little mechanistic understanding of which choice of first-line therapy is better[2]. Many centres treat patients first with targeted therapy until the tumours acquire resistance and then switch patients to immunotherapy. Interestingly, there is some clinical evidence suggesting that patients who have relapsed on targeted therapy have a lower overall response rate to immunotherapy compared to patients who are naïve to targeted therapy[7–10]. Targeted therapy resistant tumours lose CD8 T cells as determined by immunohistochemistry[11–13] and their gene expression profiles show an overlap with tumours resistant to checkpoint inhibitors[14]. Moreover, a few factors have been implicated in both, diminishing responsiveness to targeted therapy and immune evasion[15–19]. Yet whether acquired resistance to targeted therapy could jeopardize a treatment response to immunotherapy and how this could be achieved mechanistically is unknown.

Here, we provide decisive experimental evidence for the evolution of cross-resistance between targeted MAPK pathway inhibition and immunotherapy in matched, targeted therapy naïve and resistant mouse models and patients. We find that cross-resistance is mediated via an immune-evasive tumour microenvironment (TME), characterized by low abundance and impaired maturation of $CD103^+$ dendritic cells (DC). The immune-evasive TME is directly instructed by the targeted therapy resistant cancer cells. Using our lineage tracing method CaTCH[20], which allows the retrospective isolation of founding clones prior to evolutionary selection, we demonstrate that cross-resistance is acquired during MAPKi treatment. We find that cross-resistance is not a consequence of a selective bottleneck imposed by the immune system during the evolution of targeted therapy resistance, but that it arises from the enhanced transcriptional output of the MAPK pathway in targeted therapy resistant cancer cells. We identify two strategies to overcome immunotherapy resistance: (1) direct modulation of the TME via $CD103^+$ DC maturation and expansion, and (2) inhibition of the MAPK pathway that instructs the TME. Our work strongly suggests that immunotherapy should be administered before patients develop resistance to targeted MAPK pathway inhibitors and underscores the need to understand how tumours evolve during treatment response and resistance in order to identify the most potent therapeutic strategies for durable tumour control.

## Results

### Resistance to MAPKi confers cross-resistance to immunotherapy

In our melanoma patients and public datasets [7–10], we and others observed that patients have a lower response rate to immunotherapy and shorter progression-free survival when they acquired resistance to targeted therapy ($R^{TT}$) with RAF inhibitors (RAFi, e.g., vemurafenib, dabrafenib) alone or in combination with MEK inhibitors (MEKi, e.g., cobimetinib, trametinib), compared to patients who are naïve to targeted therapy ($N^{TT}$) (Fig. 1a, b; Extended Data Fig. 1a, b, Supplementary Table S1). Moreover, in $R^{TT}$ tumours, cytotoxic

$CD3^+CD8^+$ T cells and tumour-reactive $CD39^+CD103^+$ T cells that mediate anti-tumour immune-responses were reduced compared to biopsies taken from the same patient before targeted therapy, which is in line with observations in other datasets[11–13] (Fig. 1c, Extended Data Fig. 1c-e, Supplementary Table S2). These clinical correlations could suggest that $R^{TT}$ tumours do not just overcome growth restraints of oncogene inhibition by targeted therapy but simultaneously acquire immune-evasive traits.

To assess whether acquired resistance to targeted therapy could indeed impair a treatment response to immunotherapy, we modelled the evolution of targeted therapy resistance in the presence of an intact immune system in mice. We utilized two murine melanoma cell lines, one that is driven by *Braf*$^{V600E/WT}$ *Cdkn2a*$^{-/-}$ (YUMM3.3 melanoma) and one by *Braf*$^{V600E/WT}$ *Cdkn2a*$^{-/-}$ *Pten*$^{-/-}$ (YUMM1.7 melanoma). From these treatment-naive cell lines, we established $N^{TT}$ tumours in immunocompetent mice and treated them with RAFi or a RAFi/MEKi combination. Mirroring the clinical course seen in patients[1], tumours initially regressed but eventually relapsed and grew into $R^{TT}$ tumours (Fig. 1d, e). To generate matched, transplantable tumour models, we derived cell lines from $N^{TT}$ and $R^{TT}$ tumours and confirmed their sensitivity and resistance to RAFi or RAFi/MEKi (Extended Data Fig. 2a-e).

We investigated the response to immunotherapies used in the clinic, by establishing tumours from $N^{TT}$ and $R^{TT}$ cell lines of the BRAF melanoma model in immunocompetent mice and treating them with the immune checkpoint inhibitors anti-PD-1/CTLA-4. All $N^{TT}$ tumours responded to anti-PD-1/CTLA-4 in a T cell-dependent manner and regressed (Fig. 1f, Extended Data Fig. 2f-g). However, the $R^{TT}$ tumours grew unperturbed, independently of whether they were resistant to RAFi or RAFi/MEKi (Fig. 1f; Extended Data Fig. 2h). In line with these results, anti-PD-1/CTLA-4 treatment led to a 3-fold increase of $CD8^+$ T cells in $N^{TT}$, but not in $R^{TT}$ tumours (Fig. 1g, h). Importantly, these mice were never treated with RAFi or RAFi/MEKi to exclude direct drug effects for example on immune cells[21,22]. To exclude potential drug withdrawal effects on tumour cells, we exposed $R^{TT}$ tumours continuously to RAFi and also observed cross-resistance (Extended Data Fig. 2i). In summary, cross-resistance is a heritable trait of $R^{TT}$ cancer cells, which upon transplantation into mice establish immunotherapy resistant tumours.

Immunotherapies typically act by promoting T cell responses[23]. To dissect the T cell response in a well-controlled setting with a single antigen and in the presence of an equal number of antigen-specific T cells, we took advantage of the OT-1 T cell receptor/ovalbumin antigen system. We engineered the Braf/Pten melanoma model, which shows primary resistance to checkpoint inhibitors (Extended Data Fig. 3a), to present equal levels of the ovalbumin (OVA) antigen on MHC-I, making it susceptible to killing by OVA-specific OT-1 T cells (Extended Data Fig. 3b). We established $N^{TT\text{-}OVA}$ and $R^{TT\text{-}OVA}$ tumours (RAFi or RAFi/MEKi resistant) in *Rag2*$^{-/-}$ mice lacking endogenous T cells and performed adoptive T cell transfer (ACT) of luciferase-expressing effector OT-$1^{Luc}$ T cells, which are traceable by bioluminescence imaging (Fig. 2a). $N^{TT\text{-}OVA}$ tumours were rapidly infiltrated by OT-$1^{Luc}$ T cells and tumours regressed, in contrast, $R^{TT\text{-}OVA}$ tumours showed lower T cell infiltration and grew unperturbed (Fig. 2b, c; Extended Data Fig. 3c, d). In addition, $R^{TT}$ tumours continuously exposed to RAFi were also cross-resistant to ACT, excluding drug

withdrawal effects on tumour cells (Extended Data Fig. 3e-g). In conclusion, $R^{TT}$ tumours are cross-resistant to immunotherapy, even in the presence of a potent antigen and an excess of antigen-specific T cells.

## Cross-resistance is mediated via an immune-evasive TME

Cancer cells can become resistant to immunity via cell-autonomous mechanisms (e.g. loss of antigen presentation, defective IFN-γ response) or non-cell-autonomous mechanisms (e.g. by instructing an immune-evasive TME)[24]. We found a conserved IFN-γ response in $N^{TT}$ and $R^{TT}$ cells and comparable MHC-I levels and OVA peptide presentation in $N^{TT}$ and $R^{TT}$ cells, excluding the most common cell-autonomous resistance mechanisms[25](Fig. 2d, e; Extended Data Fig. 3h-k, Supplementary Table S3). Importantly, we observed that $N^{TT\text{-}OVA}$ and $R^{TT\text{-}OVA}$ cells were killed equally well in an *in vitro* co-culture assay by the same effector OT-$1^{Luc}$ T cells that failed to control $R^{TT\text{-}OVA}$ tumour growth *in vivo* (Fig. 2f, Extended Data Fig. 3l). To explore non-cell autonomous mechanisms, we probed the role of the TME in mediating cross-resistance. We experimentally exchanged the TME surrounding a minority (0.05%) of luciferase-positive, target $N^{TT\text{-}OVA\text{-}Luc}$ cells by mixing them with a majority (99.95%), thus, TME-instructing, luciferase-negative $R^{TT\text{-}OVA}$ cells (Fig. 2g). After we transferred OT-1 T cells, we tracked the survival of luciferase-positive target cells by BLI and found the $N^{TT\text{-}OVA\text{-}Luc}$ cells were shielded from OT-1-mediated killing and grew unperturbed, consistent with an immune-evasive TME established by $R^{TT\text{-}OVA}$ cells. Conversely, a minority of $R^{TT\text{-}OVA\text{-}Luc}$ cells within $N^{TT\text{-}OVA}$ tumours were eradicated by OT-1 T cells (Fig. 2h, Extended Data Fig. 3m). This was not a bystander effect due to widespread, unselective T cell killing, as 0.05% OVA-negative cells spiked into 99.95% $N^{TT\text{-}OVA}$ cells were not eradicated by OT-1 T cells (Extended Data Fig. 3n). These data indicate that $N^{TT}$ tumours establish an immune-permissive TME, whereas $R^{TT}$ tumours establish an immune-evasive TME and further suggest that $R^{TT}$ tumours can, in principle, be eradicated by T cells.

To identify the mediators of the immune-evasive TME in $R^{TT}$ tumours, we investigated the immune cell composition of the tumours, focusing first on the T cell compartment. In the Braf melanoma model we identified reduced T cell influx in $R^{TT}$ tumours (Extended Data Fig. 4a, b) and reduced T cell expansion upon checkpoint therapy (Fig. 1g, h). In the Braf/$Pten^{OVA}$ model, T cell numbers post ACT were substantially reduced in the $R^{TT}$ compared to $N^{TT}$ tumours (Fig. 3a, b). Low-input RNA sequencing (Smart-seq) revealed reduced expression of activation markers and effector molecules, such as IFN-γ, Granzyme A and B, Perforin 1, and CCL5 in T cells isolated from $R^{TT}$ tumours, indicating also a functional impairment of T cells, characteristic for a tumour with an immunosuppressive TME[26,27] (Fig. 3c, d; Extended Data Fig. 4c, d).

We found that suppressive myeloid cells, which can inhibit T cell function and have been implicated in RAFi resistance[15] were increased in $R^{TT}$ tumours of the Braf/Pten, but not the Braf melanoma model (Fig. 3e; Extended Data Fig. 4e, f). Notably, $CD103^+$ dendritic cells (DCs) were significantly reduced in $R^{TT}$ tumours of both melanoma models (Fig. 3e, f; Extended Data Fig. 4g-l). $CD103^+$ DCs have been implicated in T cell activation and recruitment and their stimulation can enhance the acute response to




Europe PMC Funders Author Manuscripts

targeted therapy and immunotherapy in melanoma[19,28–30]. Moreover, immunofluorescence staining for CLEC9a, a marker that is largely, although not exclusively, specific for this DC population in humans[31], revealed a reduction in CLEC9a$^+$ cells upon targeted therapy resistance in biopsies taken from the same patient before and after targeted therapy (Fig. 3g, Supplementary Table S2).

In Ingenuity pathway analysis of bulk tumour transcriptomes, we found that the term "DC maturation" scored as the top down-regulated pathway in $R^{TT}$ tumours (Extended Data Fig. 5a, Supplementary Table S4). To directly assess the maturation state of CD103$^+$ DCs, we isolated them from tumours and found a decreased expression of maturation markers, antigen presentation machinery, IFN-α response, and T cell stimulation and recruitment factors (e.g., IL-12b, CCL5, CXCL9, CXCL10)[32] and an increased expression of immunosuppressive factors (e.g., PTGS1/2, TGFβ, ARG1/2) in CD103$^+$ DCs from $R^{TT}$ compared to $N^{TT}$ tumours[33–35] (Fig. 3h; Extended Data Fig. 5b-d, Supplementary Table S5). Given that the maturation state of DCs is imperative for their immune-stimulatory function[36,37] we assessed the ability of CD103$^+$ DCs from $N^{TT}$ and $R^{TT}$ tumours to induce antigen-specific proliferation of naïve OT-1 T cells. Indeed, CD103$^+$ DCs isolated from $R^{TT}$ tumours failed to activate T cells and stimulate their proliferation *in vitro* (Fig. 3i, Extended Data Fig. 5e). In conclusion, the abundance and functionality of CD103$^+$ DCs are impaired in $R^{TT}$ tumours, which together with the increase in suppressive myeloid cells, may preclude a functional T cell response.

## Modulation of myeloid cells restores sensitivity to immunotherapy

To determine if therapeutic modulation of the myeloid compartment could restore the immunotherapy response in $R^{TT}$ tumours, we depleted suppressive myeloid cells, but observed tumour control only in 7 of 15 mice, likely due to rapid repopulation and high plasticity of myeloid cells (Extended Data Fig. 5f-i). To overcome the quantitative and qualitative defects of CD103$^+$ DCs and assess their contribution to cross-resistance, we induced DC expansion by expressing FLT3L in $R^{TT}$ cells and DC maturation by injecting Poly I:C into the tumours (Fig. 4a, Extended Data Fig. 5j). FLT3L-mediated DC expansion alone led to a 15-fold increase of CD103$^+$ DCs in $R^{TT\text{-}OVA}$ tumours but did not enhance T cell infiltration or induce tumour control (Fig. 4a-d; Extended Data Fig. 5k). Poly I:C mediated DC maturation enhanced T cell infiltration by inducing T cell recruitment factors such as CCL5, CXCL9, CXCL10 and was sufficient to restore tumour control (Fig. 4b-e, Extended Data Fig. 5l). CD103$^+$ DCs isolated from Poly I:C treated $R^{TT}$ tumours regained their capacity to activate T cells and stimulate their proliferation *in vitro* (Fig. 4f, g). A combination of FLT3L and Poly I:C further increased T cell infiltration and tumour control and, notably, T cell memory protected mice from tumour formation upon re-injection of $R^{TT\text{-}OVA}$ cells (Fig. 4h, i). In the second melanoma model (Braf melanoma), Poly I:C mediated DC maturation alone was also sufficient to re-sensitize $R^{TT}$ tumours to checkpoint inhibition in wild type mice. Importantly, in $BATF3^{-/-}$ mice, which lack functional CD103$^+$ DCs[19,28] tumours did not regress, demonstrating that the Poly I:C mediated re-sensitization of cross-resistant tumours is dependent on DCs (Extended Data Fig. 5m).

To investigate cross-resistance in a non-melanoma model, we used the $Kras^{G12D}$ driven murine colon carcinoma model CT26, which is responsive to MAPK pathway inhibition with MEKi. We generated matched $N^{TT}$ and MEKi-resistant $R^{TT}$ cell lines and also identified cross-resistance to anti-PD-1 in $R^{TT}$ tumours (Extended Data Fig. 6a-d). We confirmed the lack of common cell-autonomous immunotherapy resistance mechanisms and the immune-evasive TME with reduced T cell infiltration, increased suppressive myeloid cells, and reduced and immature $CD103^+$ DCs (Extended Data Fig. 6e-n). To investigate whether local, intra-tumoural DC maturation and expansion induces regressions of distant secondary tumours, we established subcutaneous $R^{TT}$ tumours at opposite flanks. Poly I:C-mediated DC maturation, in combination with FLT3 and anti-PD-1 led to complete control of the injected and the contralateral tumour (Extended Data Fig. 7a, b). This response was preceded by antigen-specific expansion of T cells in both tumours and abrogated by T cell depletion (Extended Data Fig. 7c-e). As an alternative to Poly I:C, focal radiotherapy has been described as an activator of DCs [38,39]. Indeed, combining FLT3L with radiation acted synergistically with anti-PD-1, and may represent a clinically relevant intervention strategy (Extended Data Fig. 7f, g). In summary, inducing a functional $CD103^+$ DC compartment can overcome the immune-evasive TME of $R^{TT}$ tumours and may represent a treatment strategy for cross-resistant patients.

## Cross-resistance is *acquired* and linked to the $R^{TT}$ signalling program

Understanding the mechanistic basis of cross-resistance could help to prevent or revert it. The immunosuppressive TME in $R^{TT}$ tumours is only established upon resistance to targeted therapy; whereas we noticed a remodelling of the TME[40] and increased T cell infiltration upon short term MAPK pathway inhibition in $N^{TT}$ tumours (3-7 days), consistent with previous reports [21,41,42] (Extended Data Fig. 8a, b). Thus, we investigated whether this immune cell influx could drive the evolution of cross-resistance by selecting for immune-evasive clones. However, $R^{TT}$ cell lines generated *in vitro* ($R^{TT\text{-}vitro}$) and in immunocompromised NOD/SCID gamma mice ($R^{TT\text{-}NSG}$) also displayed cross-resistance to immunotherapy, phenocopying $R^{TT}$ cells generated in immunocompetent mice (Fig. 5a-d, Extended Data Fig. 8c). Next, we investigated if cross-resistance is a general consequence of sequential therapies and generated cells resistant to dacarbazine, but these chemotherapy-resistant cells did not show cross-resistance to immunotherapy (Fig. 5e, Extended Data Fig. 8d). In summary, these data indicate that cross-resistance is mediated via a cancer cell-intrinsic program that is directly linked to MAPKi resistance and is not the consequence of selection by the immune system.

To examine whether cross-resistance is pre-existent in treatment-naïve tumours or arises during inhibition of the MAPK pathway, we used our lineage tracing tool CaTCH[20]. CaTCH allows, via diverse barcodes, the identification of $R^{TT}$ clones and can retrospectively isolate their founding $N^{TT}$ clones prior to evolutionary selection using a Cas9-VPR inducible GFP-reporter linked to the barcode (Fig. 5f). We isolated such a clonal pair and found that tumours established by the $R^{TT}$ clone showed low OT-1 T cell infiltration and grew unperturbed upon ACT, but tumours from its matched $N^{TT}$ founder clone showed high T cell infiltration and tumour regression, indicating that cross-resistance is acquired during MAPKi treatment (Fig. 5g, Extended Data Fig. 8e, f).

## The $R^{TT}$ signalling program predicts immunotherapy response

To characterize the cancer cell-intrinsic program mediating cross-resistance, we performed transcriptomic profiling of the Braf and Braf/Pten bulk tumours, as well as FACS-purified Braf/Pten melanoma cells. We identified the shared, differentially expressed genes between $N^{TT}$ and $R^{TT}$ cancer cells *in vivo*, resulting in a cancer-cell specific immune evasion signature (ccIES) that contained 106 genes and included key regulators of immune-evasion such as WNT and prostaglandin signalling (Fig. 6a, b; Extended Data Fig. 8g-i, Supplementary Table S6, S7). The ccIES was predictive for immunotherapy response in 3 independent melanoma patient cohorts[43,44], and notably, it was also prognostic in the TCGA cohort of treatment-naïve melanoma patients (Fig. 6c, d; Extended Data Fig. 8j-l). We found that the ccIES was also associated with decreased DC and T cell-specific gene signatures, altogether suggesting that $R^{TT}$ cells instruct a signalling program that is associated with an immune-evasive TME and poor response to immunotherapy (Fig. 6e; Extended Data Fig. 8m, Supplementary Table S8, S9).

## Cross-resistance is mediated via the MAPK pathway in $R^{TT}$ tumours

To identify the regulator governing the ccIES, we performed a computational upstream regulator analysis (Ingenuity) and identified MAPK signalling as the top-scoring signalling pathway (Fig. 6f). Motif analysis of the upregulated genes in the ccIES and in transcriptome data from bulk tumours also showed an enrichment of key transcription factors of MAPK signalling, such as members of the AP-1 complex (Fig. 6g, Extended Data Fig. 9a). The MAPK pathway has been implicated in immune-evasion [41,42,45]. However, intriguingly, the MAPK pathway is already active in $N^{TT}$ melanomas, suggesting that when the MAPK pathway is reactivated in $R^{TT}$ melanomas[17,46], it drives yet a *different* immune phenotype that confers immunotherapy resistance.

To investigate whether the MAPK pathway in $R^{TT}$ cells gains access to different gene regulatory regions, we assessed genome-wide alterations in chromatin accessibility in $N^{TT}$ and $R^{TT}$ cells using ATAC-seq. The top transcription factor motifs enriched in accessible chromatin of $R^{TT}$ cells were effectors of the MAPK pathway (Fig. 6h, i). We found that this enrichment stems from (1) chromatin regions that are open in $N^{TT}$ cells but are more accessible with increased activity of MAPK effectors in $R^{TT}$ cells (shared peaks) and (2) from regions, which are only accessible in $R^{TT}$ cells (unique peaks) and also enriched for motifs of central MAPK effectors (Fig. 6j). Notably, shared peaks containing no MAPK motifs displayed similar levels of accessible chromatin, indicating that the enhanced chromatin accessibility is specific for MAPK effectors (Extended Data Fig. 9b).

Next, we used SLAM-seq, a metabolic RNA labelling method for time-resolved measurement of newly transcribed (nascent) RNA, to understand whether the altered chromatin landscape changes the immediate transcriptional output of the MAPK pathway[47,48] (Extended Data Fig. 9c). We inhibited the MAPK pathway for 2h using MEKi in $N^{TT}$ and RAFi-resistant $R^{TT}$ cells, which remain responsive to MEKi, and found that 62 genes uniquely changed in $N^{TT}$, 204 in $R^{TT}$, and 222 in both $R^{TT}$ and $N^{TT}$ cells ("$N^{TT}$-specific", "$R^{TT}$-specific", and "common" targets, respectively) (Extended Data Fig. 9d-f, Supplementary Table S10). Notably, the common and $R^{TT}$-specific targets were also

transcribed at higher rates, altogether suggesting that the re-activated MAPK signalling pathway in $R^{TT}$ cells has an enhanced and altered transcriptional output (Extended Data Fig. 9g).

To address if inhibition of the enhanced MAPK pathway output is sufficient to restore responsiveness to immunotherapy, we inhibited the MAPK pathway in RAFi-resistant $R^{TT}$ tumours using MEKi (Fig. 7a). Inhibition of the MAPK pathway *in vivo* reverted the expression of 80% of the ccIES genes in RAFi-resistant $R^{TT}$ tumours, but only 12% of these genes were altered in $N^{TT}$ tumours (Fig. 7b, c). MAPK pathway inhibition in $R^{TT}$ cells led to a downregulation of mediators of immune-evasion and an upregulation of genes associated with an active immune response, such as genes in the Type-I interferon pathway (Extended Data Fig. 9h, i). Within the TME, we observed an increase of $CD103^+$ DCs and a reduction of suppressive myeloid cells (Fig. 7d). The $CD103^+$ DCs isolated from MEKi-treated $R^{TT}$ tumours showed a regained ability to activate T cells, and T cells infiltrated $R^{TT}$ tumours upon inhibition of the MAPK pathway (Fig. 7e, f; Extended Data Fig. 10a). We excluded that the TME remodelling resulted from general cell death by activating the suicide gene thymidine-kinase in $R^{TT}$ cancer cells, which led to tumour regression but not to TME remodelling (Extended Data Fig. 10b-c). Next, we combined MEKi treatment with ACT of OT-$1^{Luc}$ T cells and whereas single treatment with ACT or MEKi had no or minor effects on overall survival, the combination was strongly synergistic and led to durable tumour control in all mice (Fig. 7g; Extended Data Fig. 10d). The combination of MEKi with anti-PD-1/CTLA-4 in the RAFi resistant Braf melanoma model also significantly extended survival (Extended Data Fig. 10e).

These data indicate that $R^{TT}$ cancer cells instruct an immune-evasive TME through an enhanced MAPK pathway output, mediating cross-resistance to immunotherapy (Fig. 7h). Moreover, in our ACT model a brief treatment with targeted therapy did not interfere with subsequent T cell infiltration or tumour cell killing (Extended Data Fig. 10f-h). Although this experimental setting is highly controlled and does not test immunotherapy administration directly, taken together, our results support the notion that targeted therapy should be limited to a short period and patients should be switched to immunotherapy before resistance develops. Cross-resistance can be overcome by inhibiting the MAPK pathway or -in tumours that are resistant to MAPK pathway inhibition -by directly modulating the DC compartment to increase the efficacy of immunotherapy (Fig. 7h).

## Discussion

Tumour development relies on oncogenic signalling to initiate and maintain tumour growth and the tumour's ability to evade elimination by the immune system. Growing evidence suggests that oncogenic signalling pathways may also impair anti-tumour immune responses[49]. Consistent with this idea, the MAPK pathway in targeted therapy-naïve melanomas has been implicated in immune evasion[41,42,45]. However, despite their hyperactive MAPK pathway, the majority of targeted therapy-naive melanomas are responsive to immunotherapies[4], suggesting that hyperactivation of the MAPK pathway does not directly suppress anti-tumour immunity.

Here we show that when melanomas acquire resistance to targeted therapy, they also become resistant to immunotherapy. Cross-resistance is driven by the MAPK pathway, which is reactivated and drives resistance in the majority of targeted therapy resistant melanomas. We find that the re-activated MAPK pathway has an enhanced transcriptional output, indicated by canonical and new gene regulatory regions that are more accessible to the critical MAPK effectors of the AP-1 transcription factor complex. This enhanced transcriptional output drives immune evasion and leads to an entirely different, impaired response to immunotherapy in targeted therapy resistant tumours compared to targeted therapy-naive melanomas. We find that cross-resistance is *acquired* during MAPKi treatment, challenging the notion that resistant cells generally pre-exist before therapy (e.g. [50]). Our findings highlight that tumours can acquire a strongly immune-evasive state by modulating key oncogenic signalling pathways that initially drive tumour initiation, without the need to engage additional pathways.

The immunosuppressive TME of cross-resistant tumours is potent enough to protect cancer cells from T cell mediated killing even in the presence of a strong antigen underscoring the central role of the TME in determining therapy responses. We show that $CD103^+$ DCs are reduced and functionally impaired in the TME of $R^{TT}$ tumours in patients and mice and that restoration of DC functionality via Poly I:C-induced maturation, focal irradiation, or inhibition of the enhanced MAPK output is sufficient to restore immunotherapy responsiveness. $CD103^+$ DCs transport tumour antigens to draining lymph nodes and prime naive CD8+ T cells[29]. Moreover, they produce CXCL9/10, recruiting activated T cells to the tumour and IL-12, which boosts anti-tumour activity of T cells[28,32]. Notably, with several strategies to generate a functional DC compartment currently in clinical trials[51,52], the direct perturbation of the immune-evasive TME represents an exciting opportunity to sensitize patients to immunotherapy.

Prior studies in patients have provided correlative data suggesting cross-resistance between targeted therapy and immunotherapy. Interestingly, targeted therapy resistant tumours show reduced T cell infiltration, an increase in M2 macrophages, and a shared gene expression program with immunotherapy resistant patients[13]. Moreover, retrospective analysis of clinical studies have suggested that melanoma patients who develop resistance to targeted therapies respond worse to subsequent immunotherapies[7–10]. However, patients with acquired resistance, including patients in our own dataset, tend to have more widespread metastases, including brain metastases, and have higher LDH levels, complicating the biological interpretation of these correlative observations. Our study provides experimental evidence and mechanistic insights into the molecular basis of cross-resistance between targeted and immunotherapies, making a leap in our understanding of this clinically relevant biology. A key strength of our model systems is, for example, that targeted therapy resistant tumours can be established by implanting resistant cell lines in mice with continuous exposure to targeted therapy or in mice which have never been exposed to targeted therapies. This allowed us to show that cross-resistance is instructed by the cancer cells and does not stem from a direct, inhibitory effect of targeted therapy on immune cells. Moreover, the models allowed us to test the hypothesis whether the influx of T cells into the tumour observed in the acute response to targeted therapies, drives the emergence of cross-resistance, e.g. via immune-editing. We established tumours from targeted therapy-resistant

cell lines that were generated in immunocompromised mice and *in vitro*, where immune cells are absent, and also observed cross-resistance, ruling out immune response-induced selective pressure during resistance development as a driver of cross-resistance. Ultimately, both insights from patients and interventional experiments in mouse models are needed to reach firm conclusions about relevant disease mechanisms.

Our work has important implications for the treatment of patients, and it will influence future studies. With a large repertoire of mechanism-based therapies at hand, the future of cancer treatment lies in rational therapy combinations and the sequential administration of different treatment regimens for durable tumour control in patients. However, not even in melanoma, where both targeted and immunotherapies have been approved for years, there is a consensus on the right sequence of targeted therapy and immunotherapy[2]. Our study, together with other work[13–15,53], provides a strong scientific rationale for using immunotherapy as a first-line treatment in BRAF-mutant melanoma patients. In advanced patients, where the prompt and reliable responses of targeted therapy can be desired, patients should be switched to immunotherapy before resistance develops. Moreover, the concept of targeted therapy-immunotherapy cross-resistance we have discovered in *BRAF* mutant melanoma may also extend to other tumour types and therapies, for example *KRAS* mutant tumours. KRAS inhibitors represent a promising new treatment option and are currently in clinical trials in large patient populations with lung and colon carcinoma, which are at least in part also responsive to immunotherapies[54]. To identify effective therapeutic strategies, our work shows that it will be necessary to understand how cancer cells and their tumour microenvironment evolve through all phases of treatment, including the phase of active response and resistance to therapies.

## Material And Methods

### Ethical regulations

The research performed in this study complies with all ethical regulations. The retrospective analysis of BRAF V600 mutant melanoma patients from Lausanne University Hospital, Switzerland and was conducted in accordance with the Declaration of Helsinki, the Swiss legal requirements and the principles of Good Clinical Practice. Patients signed the CHUV General consent and accepted the use of their data for research purposes or did not explicitly refuse the use of personal data (following Art. 34 HRA). Patients did not receive compensation. The protocol was approved by the Research Ethics Committee of Canton de Vaud, Switzerland (Protocol No. 2019-00448). All experiments using animals were performed in accordance with our protocol approved by the Austrian Ministry (BMBWF-66.015/0009-V/3b/2019 or GZ: 340118/2017/25). The procedures involving irradiated animals were approved by the Animal Ethics Committee at the Institute of Cancer Research in accordance with National Home Office Regulations under the Animals (Scientific Procedures) Act 1986.

### Clinical Data

The retrospective study includes 54 BRAFV600 mutated patients treated with immunotherapy between 01.01.2011 and 29.02.2019 at the Lausanne University Hospital,

Switzerland. This cohort is divided in two groups: The targeted therapy naïve ($N^{TT}$) group refers to patients (n = 38) who received as a first line treatment immunotherapy (nivolumab, pembrolizumab or ipilimumab-nivolumab) and may have received as a second line treatment BRAF inhibitor (BRAFi, dabrafenib or vemurafenib) ± MEK inhibitor (MEKi, trametinib or cobimetinib) upon progression. The targeted therapy resistant ($R^{TT}$) group refers to patients (n = 16) who received as a first-line treatment a BRAF inhibitor (BRAFi, dabrafenib or vemurafenib) ± MEK inhibitor (MEKi, trametinib or cobimetinib) and received as a second line treatment immunotherapy (nivolumab, pembrolizumab or ipilimumab-nivolumab). The assignment of patients to the responder or non-responder groups was defined by the radiological reports of PET-CT scans and MRI scans. Responders were defined as patients with complete response (CR), partial response (PR), or stable disease (SD) of more than 3 months. Non-responders were defined as patients with progressive disease (PD) or SD for less than or equal to 3 months before disease progression. All patients were V600 BRAF-mutation positive. A detailed list of clinical characteristics and inclusion criteria is summarized in Supplementary Table S1. Survival analysis was conducted with the Kaplan–Meier method and a two-sided log-rank test was used to determine statistical significance. The association between the response and the group was investigated using a one-sided Chi-square test.

## Cell culture

Braf/Pten Melanoma (*Braf*$^{V600E/WT}$ *Pten*$^{-/-}$ *Cdkn2a*$^{-/-}$) and Braf Melanoma (*Braf*$^{V600E/}$ *Cdkn2a*$^{-/-}$) cells[55] were cultured in DMEM-F12 ; Lenti-X 293T in DMEM and CT26 colon carcinoma cells (*Kras*$^{G12D/G12D}$ *Cdkn2a*$^{-/-}$)[56] in RPMI-1640 media. All media contained 10 % FBS, 2 mM L-glutamine and 100 IU/ml penicillin/streptomycin. Primary T cells were grown in RPMI-1640 containing 10% FBS, 2 mM L-Glutamine, 100 IU/ml penicillin/streptomycin, 1 x Non-Essential Amino Acids, 1 x Sodium pyruvate, 20 mM HEPES and 0.05 mM β-Mercaptoethanol. All cells were grown at 37 °C with 5 % $CO_2$ and regularly tested negative for mycoplasma contamination. Recombinant IFN-γ (Biolegend) was administered to the cells at 10 ng/ml for 24h. $R^{TT}$ cell lines isolated from mice were continuously cultured on targeted therapy, 100 nM RAFi (dabrafenib, Selleckchem), or 100nM RAFi/30nM MEKi (trametinib, Selleckchem) for Braf/Pten and Braf Melanoma or 10 nM MEKi for CT26 colon carcinoma. To generate RAFi or RAFi/MEKi resistant melanoma or MEKi-resistant CT26 lines *in vitro*, cells were seeded at low density and exposed to 100 nM – 3 μM RAFi or 10nM – 300nM MEKi. After 6-8 weeks of continuous drug exposure, resistant cell lines were derived and cultured continuously on 100 nM RAFi, 100nM RAFi/30nM MEKi or 10nM MEKi. RAFi resistant melanoma cell lines and MEKi resistant colon carcinoma cell lines are referred to as $R^{TT}$, RAFi/MEKi double resistant cell lines are highlighted as RAFi/MEKi $R^{TT}$. To generate dacarbazine resistant cell lines, Braf melanoma cells were seeded in 50 μg/ml dacarbazine (Sigma Aldrich) for 3 -4 weeks, then concentration was increased to 100 μg/ml. All $R^{TT}$ cells were continuously cultured on treatment and resistance was confirmed using proliferation assays.

## Isolation of $N^{TT}$ and $R^{TT}$ cell lines from *in vivo* tumours

To generate cell lines from tumours, tumours were excised, cut into small pieces and dissociated for 1.5 h on 37 °C using Collagenase A (1 mg/ml, Roche) in PBS. Single cell

suspensions were strained through a 70 μm nylon mesh, washed twice in PBS and plated in complete medium containing 100 nM RAFi, 100nMRAFi/30nM MEKi or 10 nM MEKi for resistant cell lines. Cells were allowed to adhere overnight, followed by medium exchange after 16h. $N^{TT}$ and $R^{TT}$ cell line pairs were subjected to whole exome sequencing to identify mutations in cancer-associated genes that could mediate therapy resistance (Supplementary Table S11–S13).

## Plasmids and virus generation

For lentivirus production, LentiX 293T cells were transfected with 4 μg plasmid of interest, 2 μg Pax2 and 1 μg VSVG plasmid using polyethylenimine (PEI). Virus was collected 48 h, 64 h and 72 h post transfection in DMEM containing 1% FBS and used for infection in complete medium with polybrene at a concentration of 8 μg/ml. pLOBI (pRRL-SSFV-LUC2-P2a-OVA-mPGK-BLASTI-IRES-IRP720), pOBI (pRRL-SFFV-OVA-mPGK-BLASTI-IRES-IRFP), pFLTN (pRRL-SFFV-FLT3Lg-P2A-NEO), pLGP (pRRL-hU6-Luc2-GFP-PURO) and pBI7 (pRRL-BLASTI-IRES-IRP720) were used. The virus production and retroviral gene transfer of the triple-modality reporter gene TGL has been described previously (pSFG-NES-HSV1-TK/GFP/Luc)[57].

## Proliferation assay

1000 cells were plated in a 96-well plate in 100 μl medium containing vehicle control (DMSO for RAFi & MEKi; 1 M HCL for dacarbazine), RAFi, MEKi or dacarbazine at increasing concentrations. At seeding (day 0) and after 72 hours cell number was determined using a Cell-Titer Glo Assay (Promega), according to manufacturer's instructions. Luminescence read-out was performed using a Synergy H1 Plate Reader (Biotek). Fold change in proliferation was calculated relative to the day 3 vehicle control for the respective condition.

## Mouse models

For injections of Braf and Braf/Pten Melanoma 6-12-week-old male/female immune-competent B6(Cg)-$Tyr^{c\text{-}2J}$/J or male/female immune-compromised 6-24-week-old NOD.Cg-$Prkdc^{scid}$ $Il2rg^{tm1Wjl}$ /SzJ (NSG) mice were used. As recipients for ACT 6-12-week-old, male/female B6(Cg)-$Rag2^{tm1.1Cgn}$/J Ly5.2 mice [$Rag2^{-/-}$] were used. CT26 colon carcinoma cells were injected into 6-12-week-old male/female BALB/cJ. These mice were received from the in-house breeding facility and bred and housed under standard pathogen-free conditions at a housing temperature of 22 (±1) degrees, 55 (±5) % humidity and a photoperiod of 14h light, 10h dark. T cell isolation was performed from 8-20-week-old male/female OT-1 $Rag2^{-/-}$ mice, or 8-20-week-old male/female OT-1 Luc Thy1.1 mice[58]. B6.129S(C)-$Batf3^{tm1Kmm}$/J mice were purchased from Jackson laboratories and used for injection of the Braf melanoma model at an age of 6-12 weeks.

## Tumour cell injections and *in vivo* treatment studies

For subcutaneous tumour cell injections, mice were anesthetized using ketamine hydrochloride (100 mg/kg), xylazine (10 mg/kg), and acepromazine (3 mg/kg) or isoflurane and tumour cells were subcutaneously injected into the shaved flank in 50 μl of

Matrigel/PBS (1:1) (Corning). For *in vivo* resistance generation, mice were subcutaneously injected with $10^6$ cells on each flank (to increase chance of recurrence) and daily treatment by oral gavage was initiated at ~75-100 $mm^3$ tumour volume using vehicle (PBS), 30 mg/kg RAFi (dabrafenib, Tafinlar, Novartis), 1 mg/kg MEKi (trametinib, Mekinist, Novartis) or combinations of 15 mg/kg RAFi and 0.5 mg/kg MEKi. For checkpoint inhibition, 0.5 -0.7 x$10^6$ $N^{TT}$ or 0.2 -0.3 x$10^6$ $R^{TT}$ cells were injected subcutaneously in each flank and treatment with anti-PD-1 (RMP1-14 or IgG2a isotype CTRL, BioXCell; 100μg in 100μl) or anti-CTLA-4 (9D9 or IgG2b isotype CTRL, BioXCell, 100μg in 100μl) every 3 days intraperitoneally (i.p.), was initiated when tumours were palpable (day 5-6 post injection). Especially for the anti-PD-1 treatment of CT26 colon carcinoma an early treatment initiation at ~day 5-6 is essential to get reliable response to anti-PD-1 treatment. Cross-resistance phenotype in $R^{TT}$ Braf melanoma tumours receiving checkpoint blockade was confirmed both of targeted therapy (to avoid effects of drugs on the TME) and under continuous exposure to targeted therapy (5m/kg RAFi; to rule out drug withdrawal effects on cancer cells). MEKi on RAFi resistant $R^{TT}$ Braf/$Pten^{OVA}$ tumours to extract ccIES presented in Fig. 7b was initiated on day 11 in tumours injected into $Rag2^{-/-}$ mice. CTRL group was injected 3 days later, size-matched tumours were sorted after 72h of MEK inhibition. For experiments probing MEKi ± PD-1/CTLA-4 in RAFi resistant $R^{TT}$ Braf melanoma tumours, MEK inhibition was initiated on day 5 (0.5mg/kg), followed by checkpoint inhibition on day 6, 9, 12. Ganciclovir (GCV, Cymevene) to induce expression of the suicide gene Thymidine kinase was administered at 100mg/kg in PBS i.p. for 3 consecutive days, initiated at day 7. For depletion of suppressive Gr-$1^+$ myeloid cells, anti-Gr-1 depletion antibody (Clone RB6-8C5 or IgG2b isotype CTRL, BioXCell) was administered i.p. (6 μg/g) every 3 days and successful depletion was confirmed using flow cytometry on whole blood. For depletion of CD8 T cells, anti-CD8 depletion antibody (Clone 2.43 or IgG2b isotype CTRL, produced in-house, 50μg in 100μl) was administered i.p. on day 4, 7 and 12 post tumour cell injection and successful depletion was confirmed using flow cytometry on whole blood. Intratumoural Poly I:C (50 μg/tumour, high molecular weight, InvivoGen) or water control injections were initiated when tumours were palpable (day 5 -7) and repeated 3-4 days later.

## Adoptive T cell transfer

Mice were injected with a single tumour of $10^6$ Braf/Pten melanoma cells on the left flank and 4x$10^6$ pre-activated effector OT-1 T cells (see “T cell isolation and activation”) were transferred via tail vein injection when tumours reached ~100 $mm^3$ (day 6-8). Prior to ACT, cell lines were sorted as single cell clones or into stringent bulk populations to ensure equal MHC-I expression levels between $N^{TT}$ and $R^{TT}$ pairs. For Braf/$Pten^{OVA}$ 7 different $R^{TT}$ clones were profiled in ACT experiments and cross-resistance was observed in ~ 70%, which were used for follow-up experiments. Experiments involving ACT into mice bearing $R^{TT}$ Braf/$Pten^{OVA}$ were performed without administration of targeted therapy to exclude potential effects of the drug on the TME, except when indicated otherwise. To exclude effects of drug withdrawal of cancer cells, the cross-resistance phenotype and remodelled TME was also confirmed in experiments where mice were continuously kept on RAFi (10 mg/kg). TME characterization presented in Fig. 3e was performed in CTRL tumours that did not receive ACT. MEK inhibition on RAFi resistant $R^{TT}$ Braf/$Pten^{OVA}$ tumours in combination with ACT was initiated on day 6 at 0.5 mg/kg followed by ACT on day 7-8. For

BLI, anesthetized mice were injected retro-orbitally with D-luciferin (150 mg/kg, Goldbio) and imaged with an IVIS Spectrum Xenogen machine (Caliper Life Sciences).

### Tumour size monitoring

Tumour size monitoring was performed using calliper measurement every 2-4 days and calculated as: Volume = (D x $d^2$)/2, in which D and d refer to the long and short tumour diameter, respectively. For survival curves, a defined tumour volume (according to animal protocol 1000 $mm^3$ or tumour volume at first appearance of necrosis) was used as cut-off criteria across all mice in the respective experiment.

### Spike-In experiments to probe TME contribution

For “Spike-In” experiments $N^{TT}$ and $R^{TT}$ Braf/$Pten^{OVA}$ cell lines were counted, mixed at indicated ratios [0.05% (500 cells) $Luc^+$ minority population and 99.95% (999 500 cells) Luc negative, TME-instructing majority population] and subcutaneously injected into $Rag2^{-/-}$ mice. No MAPKi was applied in these experiments, to avoid drug effects on the TME or $N^{TT}$ cells. On the day of ACT, BLI imaging was performed to have a reference value of the spiked-in populations, mice were assigned into CTRL and ACT groups and ACT of $4x10^6$ pre-activated effector OT-1 T cells was performed on day 7.

### Focal radiation therapy

$3x10^5$ CT26 $R^{TT}$ cells were injected subcutaneously into the right flank of female 6-8-week-old Balb/c mice (Charles River). Animals were irradiated under anaesthesia with Hypnorm/Hypnovel (Fentanyl-Fluanisone/Midazolam), administered i.p. Irradiation was performed on day 14 using an AGO 250kV X-ray machine (AGO, Reading, UK). Radiation dose (9Gy) was measured using a Farmer Chamber and Unidos-E dosimeter. FLT3L administration was initiated on day 7 and administered in 10 consecutive doses of 30 μg i.p. (BE0098 or Isotype, BioXCell in PBS). 100 μg anti-PD-1 (RMP1-14 or IgG2a isotype CTRL, BioXCell) were administered on day 15, 18, 21 and 24. Body weight and tumour growth were measured twice weekly and tumour volumes calculated as: length x width x height (mm) x 0.5236.

### CRISPRa Tracing of Clones in Heterogeneous cell populations (CaTCH) experiments

All experiments involving CaTCH were performed as previously described in ref[20]. Purity of CaTCH isolated matched $N^{TT}$ and $R^{TT}$ clones was confirmed by next generation sequencing of their barcode sequence and matching $N^{TT}$ and $R^{TT}$ cell lines were infected with pOBI (pRRL-SFFV-OVA-mPGK-BLASTI-IRES-IRFP). For ACT experiments OVA infected bulk populations were used. ACT of pre-activated OT-1 Luc T cells was performed on day 7 post injection, as described in “in vivo studies”.

### T cell isolation and activation

T cell isolation was performed using the naïve $CD8^+$ T cell isolation kit (Miltenyi Biotec). Spleens and mesenteric lymph nodes were isolated from donor mice and processed according to the manufacturer’s protocol. Naïve $CD8^+$ T cells were then either used directly

or activated with anti-CD3 (2 μg/ml) and anti-CD28 (1 μg/ml) (both eBioscience) for 16 h and expanded for 6 days in IL-2 (15 ng/ml, in-house produced).

### *In vitro* T cell killing assay

$2x10^4$ $OVA^+$ cancer cells were seeded into 24-well plates and allowed to attach overnight. Pre-activated, effector OT-1 T cells were then seeded onto the cancer cells in indicated effector: target ratio (accounting for one doubling overnight) in complete T cell medium containing IL-2 (15 ng/ml). After 24 hours of co-culture, remaining cells were stained with CD8a and DAPI as a live/dead marker and analysed by flow cytometry. $OVA^-$ cancer cells were used as a specificity control for killing.

### *In vitro* DC co-culture assay

For $CD103^+$ DC isolation, tumours (derived from $Braf/Pten^{OVA}$ melanoma bearing Rag2-/- mice) were dissected, cut into small pieces and dissociated for 1.5 h on 37 °C using Collagenase A (1 mg/ml, Roche) in PBS. In case of experiments profiling the effect of MEKi on the DC compartment, mice received 3 doses of MEKi (0.5 mg/kg) prior to DC isolation. In case of experiments profiling the effect of Poly I:C on the DC compartment, mice received 2 doses of Poly I:C prior to DC isolation (24h after the second dose). Single cell suspensions were strained through a 70 μm nylon mesh, washed in FACS buffer (0.5 % BSA, 2 mM EDTA) and incubated for 10 min on 4°C with anti-mouse Fc-Block CD16/CD32 antibody. Cells were stained with biotinylated anti-CD103 (clone REA789, Miltenyi Biotec) and isolation of labelled $CD103^+$ cells was performed with anti-biotin microbeads (Miltenyi Biotec), according to the manufacturer's protocol, and purity was confirmed using flow cytometry for MHCII eF450. For co-culture 150,000 naïve OT-1 CFSE labelled (0.25 μM, Thermo Fisher) T cells were co-cultured with 50,000 freshly isolated $CD103^+$ DCs in a 96 well plate in complete T cell medium. After 72h, the cell suspension was stained with a live/dead marker and CD3e-BV605. The proliferation of OT-1 T cells was determined based on CFSE dilution. As a positive control naïve OT-1 CFSE labelled T cells were activated with anti-CD3 (2 μg/ml) and anti-CD28 (1 μg/ml) (both eBioscience) for 16 h and expanded for 3 days in IL-2 (15 ng/ml, in-house produced).

### Flow cytometry

For flow cytometry of whole tumours, tumours were dissected, cut into small pieces and dissociated for 1.5 h on 37 °C using Collagenase A (1 mg/ml, Roche) in PBS. Single cell suspensions were strained through a 70 μm nylon mesh, washed in FACS buffer (0.5 % BSA, 2 mM EDTA) and incubated for 10 min on 4°C with anti-mouse Fc-Block CD16/CD32 antibody. Cells were subsequently stained with antibodies detecting immune cells in FACS buffer for 30 min on 4°C. Cells were washed twice in PBS and live-dead exclusion was performed using DAPI staining or fixable viability dye eF780 (eBioscience, 1: 1000). $CD103^+$ DCs were defined as $CD103^+CD11c^+$ out of alive, singlet $CD45^+$ cells. $CD103^+$ $CD11^+$ DCs were also gated as $CD103^+MHCII^+$ out of alive, singlet $CD45^+$, lineage negative ($CD11b^-$, $Gr\text{-}1^-$, $NK1.1^-$, $B220^-$, $CD3^-$, $F/480^-$) cells, which resulted in similar ratios between $N^{TT}$ and $R^{TT}$. For the Braf/Pten and Braf melanoma model, suppressive myeloid cells were defined as $CD11b^+Gr1^+$ out of alive, singlet $CD45^+$ cells, for CT26 model as $CD11b^+Ly6C^+$ or $CD11b^+Gr1^+$ out of alive, singlet $CD45^+$ cells. Staining for H2-

$L^D$-restricted MuLV gp70-specific $CD8^+$ T cells was performed according to manufacturer's instructions on bulk tumours using H2-$L^D$ -MuLV gp70 tetramer, CD8-FITC and fixable viability dye eF780 (eBioscience, 1: 1000). All antibody information can be found in the Reporting summary.

For flow cytometry of cultured cells, cells were detached using 0.05% Trypsin, inhibited with complete medium and stained in FACS buffer (0.5% BSA, 2mM EDTA) for 30 min on 4°C. Cells were washed twice in PBS and live-dead exclusion was performed using DAPI staining or fixable viability dye eF780 (eBioscience, 1: 1000). Data was acquired using a BD LSR Fortessa and analysed using FlowJo 10.7.1. For sorting of stained samples, a BD Aria machine was used.

### Immunoblotting

RIPA buffer containing protease and phosphatase inhibitors (CST, Thermo Fisher) was used according to manufacturer's instructions. Protein concentrations were determined using BCA Protein Assay Kit (Pierce). Proteins were separated using a 4-12 % gradient Bis-Tris polyacrylamide gel in the MOPS buffer system (Invitrogen) and transferred onto nitrocellulose membranes (Bio-Rad) using standard protocols. Membranes were blocked in 5% milk and incubated with antibodies in 5% milk overnight on 4°C (for antibody information see Reporting summary). After primary antibody incubation and washing, membranes were probed with HRP-coupled secondary antibodies (1:5000 in 5% milk) and developed using the ECL system (GE Healthcare).

### Immunofluorescence staining murine tumours

Tissues for immunofluorescence staining of tumours were obtained after fixation in 4 % PFA on 4 °C and two subsequent dehydration steps from 15 % sucrose to 30 % sucrose. Tumours were then sliced using a sledge microtome and slices (30 µm) were blocked in 10 % goat serum, 2 % BSA, 0.25 % Triton in PBS for 2 h at room temperature (RT). Primary antibodies (see Reporting summary) were incubated overnight in the blocking solution at 4°C and on the next day for 30 min at RT. After 5 washes in PBS/0.25 % Triton, secondary antibodies were added for 1 h on RT at a concentration of 1:1000 followed by 5 additional washes. Then, nuclei were stained with Hoechst solution (Thermo Fisher), tumour slices were washed twice with PBS, transferred onto glass slides and mounted with Prolong Gold anti fade reagent (Thermo Fisher). For quantification of IF stainings, 5 room of interest (ROI) were acquired per tumour and counted manually using ImageJ. Margin was defined as 300 µm from tumour border and centre was defined as ~ 1mm from tumour margin onwards. For each condition ≥2 tumours with each ≥5 ROIs were counted.

### Immunofluorescence staining melanoma patient biopsies

Patient biopsies from a cohort of 10 patients prior to ($N^{TT}$) and after progression on MAPK pathway inhibitors (BRAFi or BRAFi/MEKi combination therapy, $R^{TT}$) were processed for multiplex immunofluorescence staining (Supplementary Table S2). Formalin-fixed paraffin-embedded (FFPE) melanoma biopsies were cut into 3 µm sections and mounted on Superfrost Plus slides (Thermo Scientific). FFPE slides were heated in the oven at 65 °C for 30 minutes, deparaffinized in xylene (5 min in 2 x xylene) and rehydrated in ethanol (5 min

in 2 x 100% ethanol, 5 min in 1 x 95% ethanol, 5 min in 70% ethanol). Antigen retrieval was performed in AR9 buffer (Akoya; AR900) at 110 °C for 10 min in a pressurized decloaking chamber (Biocare Medical, Concord, CA). Slides were cooled in a flowing water bath for 5 minutes before commencing staining using an automated slide stainer (intelliPATH FLX, Biocare Medical). Tissue sections were blocked with 3% hydrogen peroxide in TBST for 5 minutes. Primary antibodies (see Reporting summary) were incubated for 30 minutes. Primary antibodies were detected with Opal Polymer HRP Ms + Rb for 30 minutes and visualized using Tyramide Signal Amplification with 10-minute incubations (Opal 7-Colour IHC, Akoya, USA; CD103 Opal 520, CD8 Opal 570, CD3 Opal 620, CD39 Opal 650, SOX10 Opal 690). Between subsequent staining runs, the sections were decloaked in pH 9 AR buffer in the decloaking chamber at 110°C for 10 minutes to strip the antibody-HRP complex from the samples. Sections were counterstained with DAPI (2 drops in 1mL) for nuclei visualization, and subsequently coverslipped using ProLong Diamond Antifade Mountant (Invitrogen).

For CLEC9a staining on patient biopsies, stainings were performed using the Alexa Fluor 488 Tyramide SuperBoost Kit (Thermo Scientific, B40922). In brief, biopsies were dewaxed, antigen retrieval was performed in EDTA (pH=8.5), slides were blocked in 3% hydrogen peroxide for 10 min in the dark, followed by 3 washing steps in TBS-T and blockade in 10% goat serum for 30 minutes. Slides were stained with primary antibody (see Reporting summary) for 1 hour at RT, followed by 3 washes in TBS-T and incubation with secondary antibody (goat-anti-rabbit Poly HRP, Thermo Scientific, B40922) for 1h at RT. Slides were washed 3 times in TBS-T and incubated with Tyramide 488 working solution for 12min at RT. Stop solution was applied, followed by 3 washes in TBST and elution. Slides were counterstained with DAPI, cover slipped and mounted in ProLong Diamond Antifade Mountant (Invitrogen).

### Image analysis melanoma patient biopsies

Sections were imaged using Vectra 3.0 multispectral imaging system (Akoya). A spectral library with appropriate fluorescent filters (cy3 for Opal570, Texas Red for Opal620, cy5 for Opal650 and Opal690, FITC for Opal520, and DAPI) was used for multispectral analysis. A whole slide scan on the multiplex tissue sections produced multispectral fluorescent images visualized in Phenochart, from which tumour regions were outlined and selected for imaging high-power 20x multispectral images (MSI) for further analysis. Analysis of the MSIs was conducted using InForm image analysis software (Akoya). The multispectral images were unmixed in inform2.3 (Akoya) and exported as qtiff images. These qtiff images were fused into one image and images were imported into HALO 3.0.311.261 (Indicia labs) to quantify the expression of above markers on a cell by cell basis. The software was first trained to distinguish between tumour, stroma and blank slide areas within the melanoma samples, then to segment the tissue categories into the cell components: the nuclei, cytoplasm and membrane of each cell. The positivity threshold of each marker was determined and recorded for further data analysis. Once the algorithm was completed, all samples were run as a batch. To ensure effective segmentation of the samples, thresholds were examined post-analysis and reviewed, and the algorithm was either adjusted or separate algorithms were created for variable staining across the samples. The quantitative analysis

was performed using TIBCO Spotfire 3.3.1.1. For quantifications displayed in Fig 1.c and Extended Data Fig. 1e tumour and stroma were averaged across each patient. For quantifications of CLEC9a positive cells, slides were scanned using Pannoramic 250 (3D Histech) and counting was performed manually on 10 ROIs per tumour. Average cell number across 10 ROIs in matched $N^{TT}$ and $R^{TT}$ biopsies is reported in Fig. 3g.

### SLAM-seq sample preparation

Braf/$Pten^{OVA}$ $N^{TT}$ and $R^{TT}$ cells were seeded, allowed to adhere overnight and medium was replaced with complete medium (10% FBS to activate signalling and induce a transcriptional response mimicking growth-factor rich environments) containing vehicle (DMSO) or MEKi (100nM trametinib) the next morning (cell density did not exceed 60-70% confluency). 30 min after drug addition, 4-SU (Carbosynth) was added at a final concentration of 100 μM. Newly synthesized RNA was labelled for 90 mins. Cells were harvested by direct snap-freezing of plates on dry ice. RNA extraction was performed using the RNAeasy Plus Mini Kit (Qiagen) and total RNA was subjected to alkylation by iodoacetamide (Sigma, 10mM) for 15 min and RNA was re-purified by ethanol precipitation[47,48]. 500ng RNA was used as input for generating 3' end mRNA sequencing libraries using the Lexogen Quant-seq 3'mRNA-Seq library prep kit FWD for Illumina. Sequencing was performed in-house using NextSeq550 to obtain single-end 150bp reads.

### SLAM-seq data analysis

Analysis of SLAM-seq data is described in the Reporting summary.

### Sample preparation for gene expression analysis

Whole RNA was isolated from cells using RNAeasy Mini Kit (Qiagen). For RNA isolation from bulk tumours, tumours were homogenized in Trizol and RNA was extracted using chloroform, followed by a clean-up step using the RNAeasy Mini Kit. For standard RNA-seq, libraries were generated using the Lexogen sense mRNA seq library kit using 500 ng – 1 μg of input RNA, for Quant-seq libraries were generated using the Lexogen Quant-seq 3' mRNA seq kit using 500 ng input RNA, both according to manufacturer's instructions. All libraries were quality controlled on a fragment analyser and quantified using the Qbit HS dsDNA kit (Thermo Scientific). Smart-seq analysis of 100 sorted DCs ($DAPI^-$ $CD45^+$ $CD11c^+$ $CD103^+$) or 100 sorted T cells ($DAPI^-$ $CD45^+$ $CD3e^+$ $CD8a^+$) was performed in-house using the Smart-seq2 protocol by Illumina[59]. Library prep was performed according to manufacturer's instruction using the Nextera kit after direct sorting into RNA lysis buffer. Sequencing was performed in-house on Illumina HiSeqV4 to obtain 50 bp single-end sequencing reads.

### Gene expression analysis

Gene expression analysis is described in the Reporting summary.

### ccIES signature generation

To generate the ccIES expression signature, we compared $R^{TT}$ vs. $N^{TT}$ bulk transcriptomic data for Braf melanoma and Braf/Pten melanoma tumours and extracted genes consistently

deregulated in both models with FC <−1.5 or >1.5 and padj <0.05 (IES, immune evasion signature = 279 genes, Supplementary Table S6). From these 279 genes, we sub-setted to genes deregulated in sorted cancer cells of the Braf/Pten$^{OVA}$ melanoma model from untreated tumours out of Rag2$^{-/-}$ and included genes with LFC <−1 or >1 and padj <0.05 when comparing R$^{TT}$ vs. N$^{TT}$ (Supplementary Table S7). We also confirmed the expression of the ccIES signature in R$^{TT}$ tumours continuously treated with RAFi (10 mg/kg) excluding potential effects of drug withdrawal and in tumours resistant to the combination of RAFi/MEKi.

## ATAC-Seq sample preparation

ATAC-seq was performed according to an adapted version adapted version of the Omni-ATACseq protocol[60]. Briefly, nuclei were isolated with nuclei isolation buffer (0.32 M sucrose, 3 mM CaCl2, 2 mM Mg Acetate, 0.1 mM EDTA, 10 mM Tris.HCl pH 8.0, 0.6% NP-40, 1mM DTT). After isolation, approximately 50,000 nuclei were resuspended in TD buffer with the Illumina Tn5 transposase (#15027865). The transposition reaction was performed at 37°C for 30 min. DNA fragments were purified from the reaction with the MinElute PCR purification Kit, Qiagen (# 28006) and amplified using the NEB Q5 High Fidelity PCR Mix (#M0492). Library quality was assessed using a Fragment Analyzer system (Agilent). ATAC-seq libraries were quantified using a KAPA library quantification kit and sequenced on a NovaSeq instrument in 50 bp paired-end mode.

## ATAC-seq data analysis

ATAC-seq data analysis is described in the Reporting summary.

## Whole Exome Sequencing (WES) and Analysis

Genomic DNA was isolated from frozen cell pellets with the use of DNeasy Blood & Tissue kit (Qiagen). Library preparation and sequencing was performed by Macrogen, Inc. using the Agilent SureSelect Murine All Exon Library and NovaSeq 6000 with 2 x 150 bp and at least 50x on-target coverage. Data analysis is described in the Reporting summary. WES results are shown in Supplementary Tables 11-13.

## Statistics and reproducibility

Data are displayed as mean ± SEM. All samples meeting proper experimental conditions were included in the analysis. In mouse experiments, mice that had to be euthanized due to necrotic tumours were excluded. For Smart-seq experiments, 2 samples for CD103$^{+}$ DCs and 3 samples for T cells were excluded due to poor library quality. For image quantification one tumour of the Braf melanoma model was excluded due to necrosis. No statistical method was used to predetermine sample size, group sizes were determined based on results of preliminary experiments. Group allocation was performed in a randomized fashion. The investigators were not blinded to allocation during outcome assessment. Phenotype defining experiments were repeated by independent investigators. Normality was tested using the D'Agostino–Pearson test for n > 7; otherwise, Shapiro–Wilk was used. F test was used to assess the equality of variances. Statistical significance was determined using two-sided unpaired T-test for normal distributed datasets with equal variance, Welch

correction was performed for samples with unequal variance. Two-sided Mann-Whitney U test was performed for datasets without normal distribution, one-way ANOVA was used for comparison of more than two samples and two-way ANOVA was used to analyse tumour growth over time. Two-sided log-rank test was performed to analyse survival for categorical variables. For testing the association of continuous gene scores with patient survival Cox proportional hazards models were used. Correlation between gene scores was tested using Pearson's correlation. Prism software (Graphpad, v7 and v8.3.1) and R were used for all statistical analysis. Significance was set to * $P < 0.05$, ** $P < 0.01$, *** $P < 0.001$, *** $P < 0.0001$. Replication experiments were successful and the number of replications for each experiment is listed in the figure legends. Further information on research design is available in the Nature Research Reporting Summary linked to this article.



Europe PMC Funders Author Manuscripts

## Extended Data

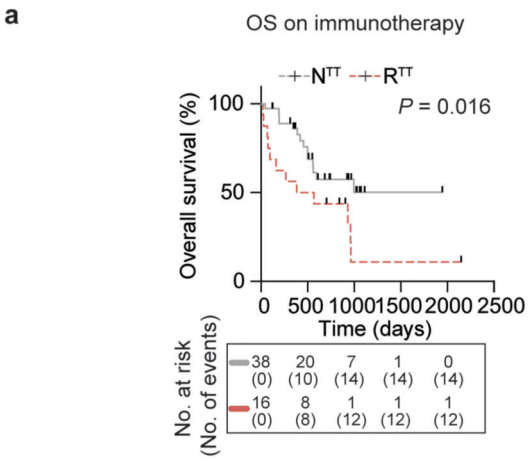


**b**

| Clinical response to immunotherapy | | $N^{TT}$ | $R^{TT}$ |
|---|---|---|---|
| Mason *et al.* 2019, anti-PD-1/CTLA-4 | PFS, months | 11 | 2 |
| | ORR, % | 57 | 21 |
| Tetu *et al.* 2018, anti-PD-1/CTLA-4 | PFS, months | 15.1 | 2.5 |
| | ORR, % | 58 | 35 |
| Johnson *et al.* 2017, anti-PD-1 | PFS, months | 10.6 | 2.8 |
| | ORR, % | 41 | 25 |
| Ackerman *et al.* 2014, anti-CTLA-4 | PFS, months | 6.7 | 2.7 |

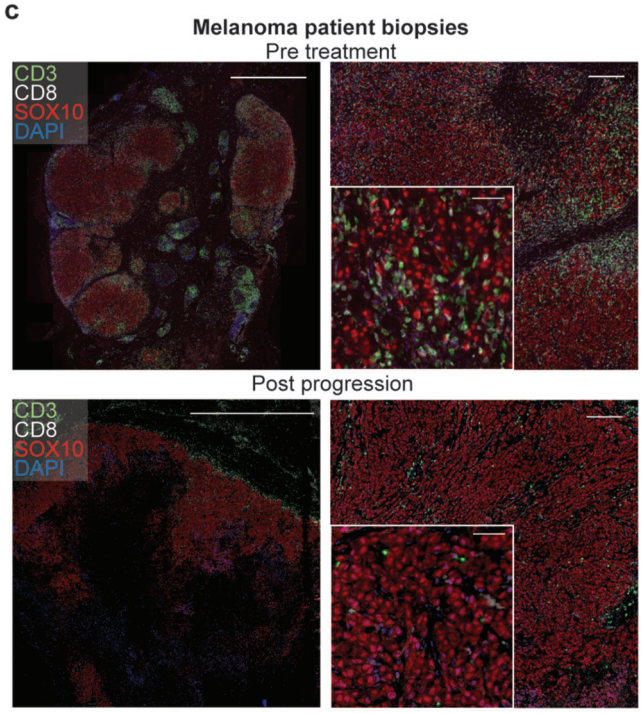


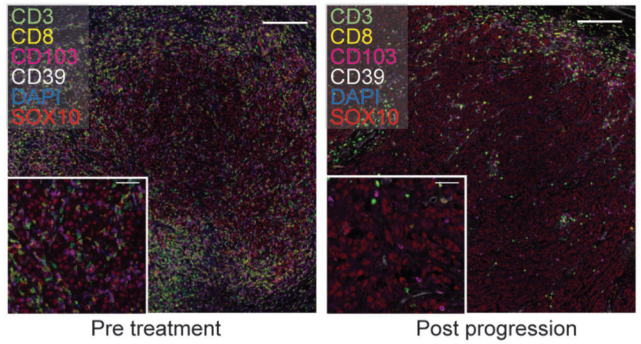


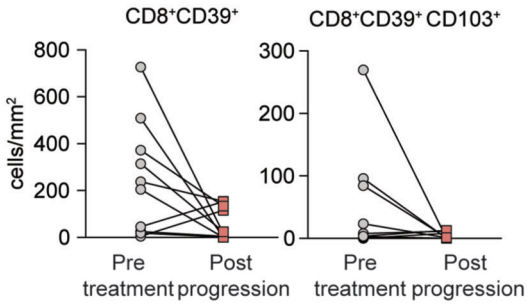


**Extended Data Fig. 1. Targeted therapy resistant patients display reduced T cell infiltrate and cross-resistance to immunotherapy.**

**a,** Overall survival (OS) of metastatic melanoma patients in the Lausanne Patient Cohort (Supplementary Table S1) receiving immunotherapy with checkpoint inhibitors ($n = 54$ patients). $N^{TT}$, targeted therapy (TT) naïve patients ($n = 38$); $R^{TT}$, TT (RAFi or RAFi/MEKi) resistant patients ($n = 16$). **b,** Summary of responses to immunotherapy in $N^{TT}$ and $R^{TT}$ patients in published patient cohorts (ORR = overall response rate, PFS = progression-free survival). **c,** $CD3^+CD8^+$ T cells in patient-matched $N^{TT}$ and $R^{TT}$ melanoma biopsies [scale bar pre-treatment: 2mm (left), 200 μm (right), 50μm (zoom-in); scale bar post progression: 5mm (left), 200 μm (right), 50μm (zoom-in)]. Experiment performed

once on 10 matched biopsies. **d,** $CD8^+CD39^+CD103^+$ T cells in patient-matched $N^{TT}$ and $R^{TT}$ melanoma biopsies [scale bar: 200 μm, 50μm (zoom-in)]. **e,** Quantification of tumour reactive ($CD8^+CD39^+CD103^+$) T cells in patient-matched $N^{TT}$ and $R^{TT}$ melanoma biopsies, assessed by IF staining ($n$ = 10 patients, Supplementary Table S2). Data analysis **a** two-sided log-rank (Mantel-Cox) test.

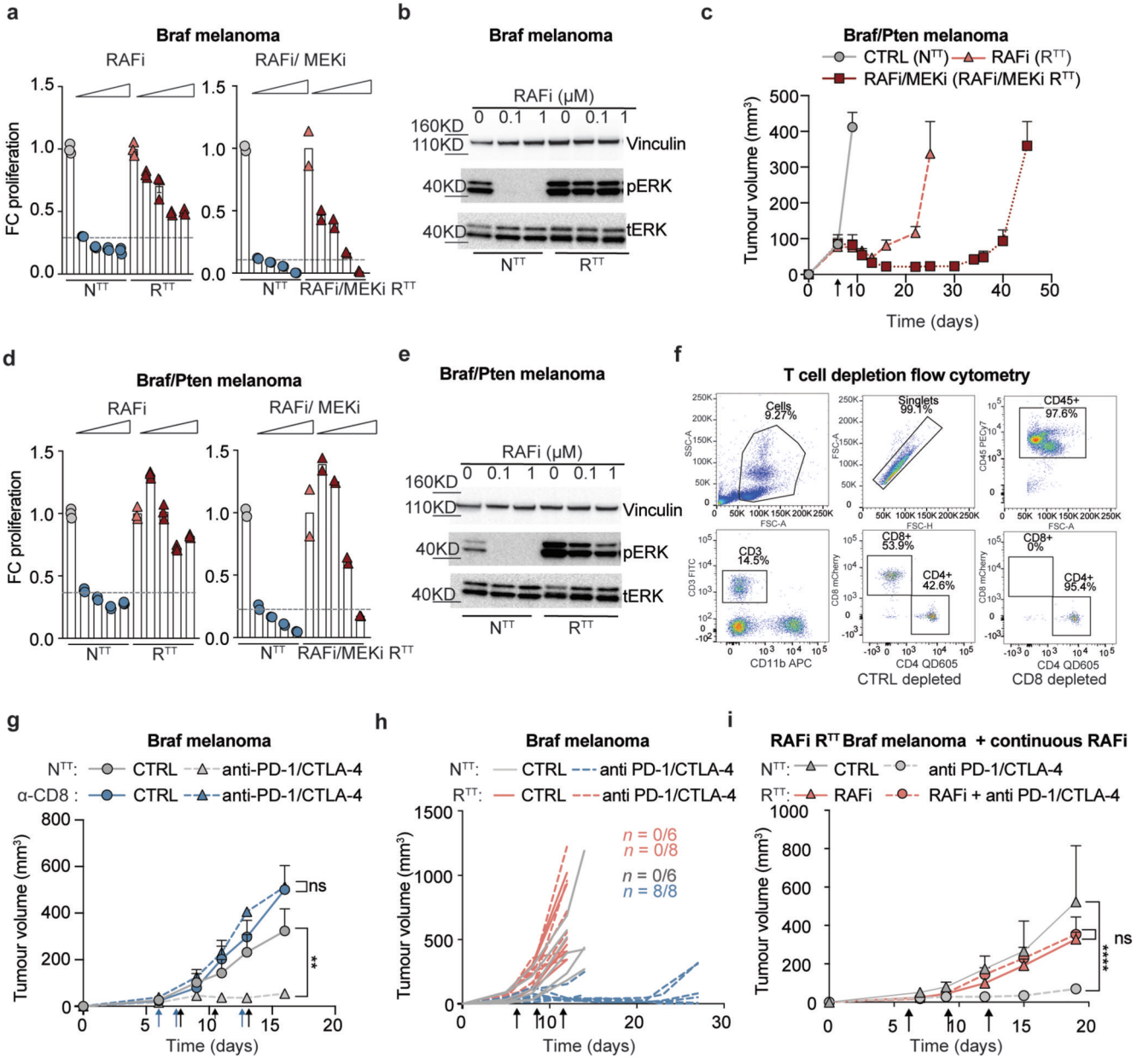


**Extended Data Fig. 2. The Braf melanoma model responds to checkpoint inhibition in the $N^{TT}$ state, but is resistant in the $R^{TT}$ state.**

**a,** Proliferation fold change (FC) of Braf melanoma cells after 72h at indicated drug conditions. Line indicating FC in proliferation of $N^{TT}$ cells on lowest drug condition ($n$ = RAFi: technical triplicates; RAFi/MEKi technical duplicates), (drug concentrations:

RAFi: DMSO CTRL, 100nM, 300nM, 1μM, 3μM; RAFi/MEKi: DMSO CTRL, 10nM/3nM, 30nM/10nM, 100nM/30nM, 300nM/100nM). **b,** pERK status in $N^{TT}$ and $R^{TT}$ Braf melanoma cells, 1-hour post drug exposure. Experiment performed twice; representative example shown. **c,** Treatment response of subcutaneously injected Braf/Pten melanoma (CTRL, $n = 4$ tumours; other groups, $n = 6$ tumours) continuously treated with TT; arrow indicating start of therapy. Experiment repeated 5 times; representative example shown. **d,** Proliferation FC of Braf/Pten melanoma cells after 72h at indicated drug conditions. Line indicating FC in proliferation of $N^{TT}$ cells on lowest drug condition ($n =$ RAFi: technical triplicates; RAFi/MEKi technical duplicates), (drug concentrations: RAFi: DMSO CTRL, 100nM, 300nM, 1μM, 3μM; RAFi/MEKi: DMSO CTRL, 10nM/3nM, 30nM/10nM, 100nM/30nM, 300nM/100nM). **e,** pERK status in $N^{TT}$ and $R^{TT}$ Braf/Pten melanoma cells, 1-hour post drug exposure. Experiment performed twice; representative example shown. **f,** Gating strategy highlighting successful CD8 T cell depletion in blood of mice treated with anti-CD8 versus CTRL antibody. **g,** Treatment response to anti-PD-1/CTLA-4 in combination with CD8 depletion in Braf melanoma. (CTRL, $n = 6$; all other groups, $n = 10$ tumours). Black arrows indicate anti-PD-1/CTLA-4 administration and blue arrows administration of CD8 depletion antibody. Experiment performed once. *P*-value: ** 0.0012, ns 0.9970. **h,** Spider plots indicating individual tumour growth curves of $N^{TT}$ and $R^{TT}$ Braf melanoma receiving checkpoint blockade (CTRL $n = 6$ tumours; anti-PD-1/CTLA-4, $n = 8$ tumours). Experiment repeated 9 times; representative example shown. **i,** Treatment response to anti-PD-1/CTLA-4 of $N^{TT}$ and $R^{TT}$ Braf melanoma (CTRL, RAFi $n = 6$ tumours; anti-PD-1/CTLA-4 ± RAFi, $n = 10$ tumours); arrows indicate therapy administration. $R^{TT}$ mice continuously treated with RAFi (5 mg/kg). Experiment performed once. *P*-value: **** 8.4e-6, ns 0.9924. Data in **a, c, d, g, i** displayed as mean ± SEM. Data analysis **g, i** two-way ANOVA. ** $P < 0.01$, **** $P < 0.0001$, ns = non-significant.

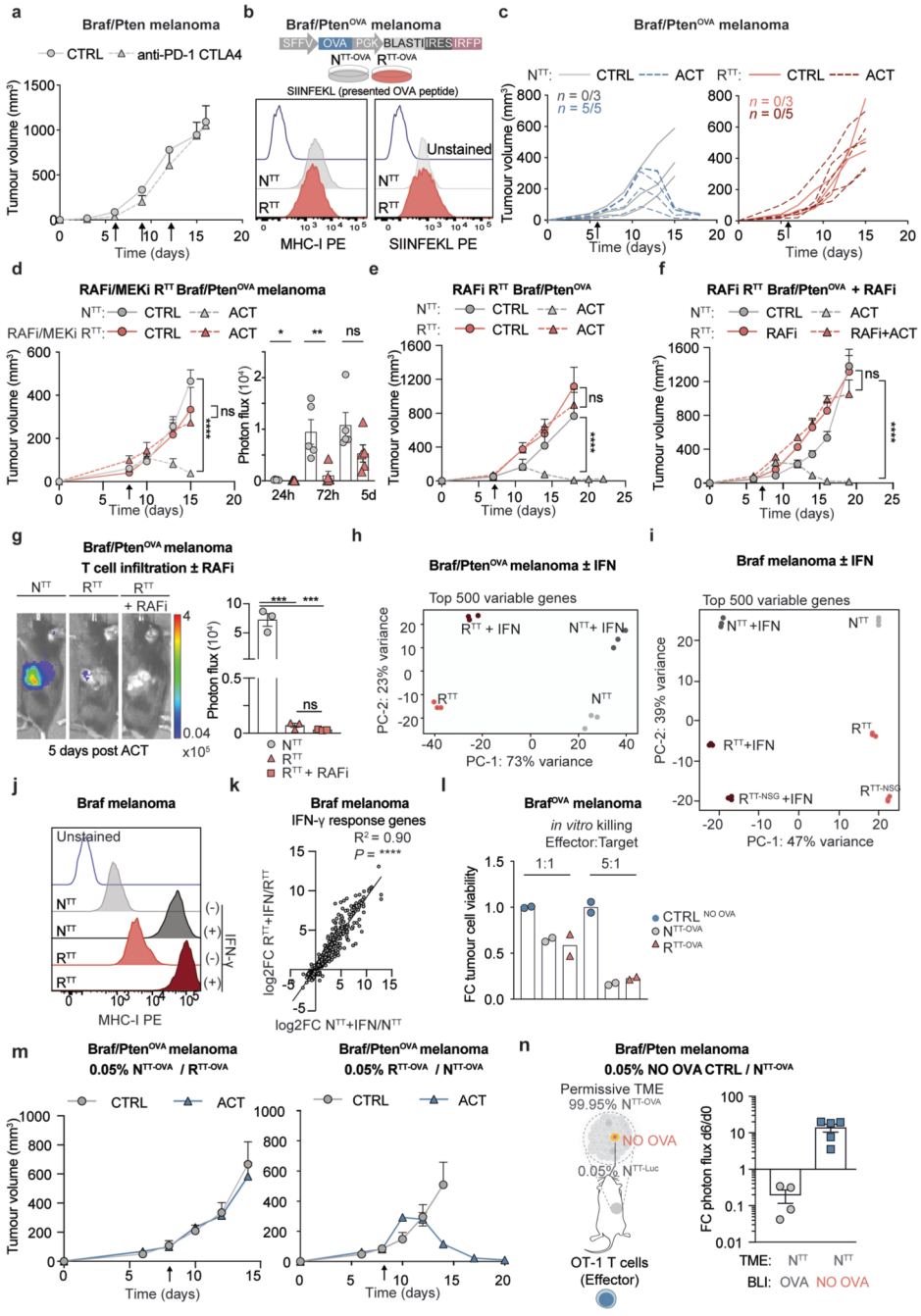


**Extended Data Fig. 3. Cross-resistance is mediated via the tumour microenvironment.**

**a,** Treatment response to immunotherapy in $N^{TT}$ Braf/Pten melanoma tumour bearing mice, black arrows indicate therapy administration ($N^{TT}$ CTRL, $n = 2$; $N^{TT}$ anti-PD-1/CTLA-4, $n = 4$ mice). Experiment performed once. **b,** Generation of OVA antigen-expressing $N^{TT}$ and $R^{TT}$ Braf/Pten cell lines using indicated expression vector (top) and quantification of processed MHC-I loaded ovalbumin peptide (SIINFEKL) by flow-cytometry (bottom). **c,** Spider Plots indicating individual tumour growth curves of $N^{TT}$ and $R^{TT}$ Braf/Pten$^{OVA}$ tumours receiving ACT (CTRL $n = 3$; ACT, $n = 5$ tumours). Experiment performed 7

times; representative example shown. **d,** Treatment response to ACT in RAFi/MEKi $R^{TT}$ Braf/Pten$^{OVA}$ tumours; arrow indicating day of ACT ($N^{TT}$, RAFi/MEKi $R^{TT}$ CTRL, $n = 3$ mice; $N^{TT}$, RAFi/MEKi $R^{TT}$ ACT, $n = 5$ mice, *P*-value: **** 3.9E-11, ns 0.6) (left) and infiltration of OT-1$^{Luc}$ T cells measured by bioluminescence imaging (BLI) at indicated days (all groups, $n = 5$ tumours *P*-value: * 0.021, ** 0.0079, ns 0.0952) (right). Experiment performed twice with two independent clones; representative example shown. **e, f,** Treatment response to ACT in Braf/Pten$^{OVA}$ tumours, $R^{TT}$ tumours assessed **(e)** off RAFi for the entire experiment [*P*-value: **** 1.7E-6, ns 0.33] and **(f)** under continuous exposure to RAFi (10 mg/kg) [*P*-value: ****5.8E-8, ns 0.35]; arrow indicating day of ACT ($N^{TT}$, $R^{TT}$ CTRL, $n = 3$ mice $N^{TT}$, $R^{TT}$ ACT, $n = 5$ mice). **g,** Tumour infiltration of OT-1$^{Luc}$ T cells into $N^{TT}$ Braf/Pten$^{OVA}$ tumours and $R^{TT}$ Braf/Pten$^{OVA}$ tumours ± RAFi (10 mg/kg), (all groups, $n = 3$ mice). Experiment performed once. *P*-value: *** 0.0004, *** 0.0003. **h, i** Principal Component Analysis (PCA) plots displaying top 500 most variable genes for **(h)** Braf/Pten and **(i)** Braf melanoma treated with IFN-γ. **j,** MHC-I surface expression of $N^{TT}$ and $R^{TT}$ Braf melanoma cell lines (baseline and 24h post 10 ng/ml IFN-γ exposure). Experiment performed 3 times; representative example shown. **k,** Gene expression changes in $N^{TT}$ and $R^{TT}$ Braf melanoma cell lines treated with IFN-γ. Correlation between genes deregulated in $N^{TT}$ (x-Axis) and $R^{TT}$ (y-Axis) cell lines ($P < 0.05$), dots display individual genes. *P*-value: <1E−15. Supplementary Table S3. **l,** Braf$^{OVA}$ melanoma cell viability after 24 h of co-culture in *in vitro* killing assay using pre-activated OT-1 T cells at indicated effector:target ratios (all groups, $n = 2$ replicates). Experiment performed twice; representative example shown. **m,** Treatment response to ACT in tumours consisting of $N^{TT}$ and $R^{TT}$ Braf/Pten$^{OVA}$ cell lines at indicated ratios; arrow indicating day of ACT (0.05% $N^{TT}$/$R^{TT}$ CTRL, $n = 4$; ACT, $n = 5$; 0.05% $R^{TT}$/$N^{TT}$ CTRL, $n = 4$; ACT, $n = 4$ tumours). Experiment performed twice; representative example shown. **n,** Scheme outlining experiments to test antigen-specificity of T cell killing *in vivo* (left) and BLI signal at day 6 post ACT for tumours containing 0.05% $OVA^+$ $Luc^+$ or 0.05% $OVA^-$ $Luc^+$ CTRL cells ($N^{TT}$/ $OVA^+$ $n = 4$; $N^{TT}$/ $OVA^-$ CTRL $n = 5$ tumours) (right). Data in **a, d-g, m, n** displayed as mean ± SEM. Data analysis **d-f** two-way ANOVA **d** two-tailed unpaired t-test **g** one-way ANOVA **k** two-sided Pearson correlation. * $P < 0.05$, ** $P < 0.01$, *** $P < 0.001$, **** $P < 0.0001$, ns = non-significant.

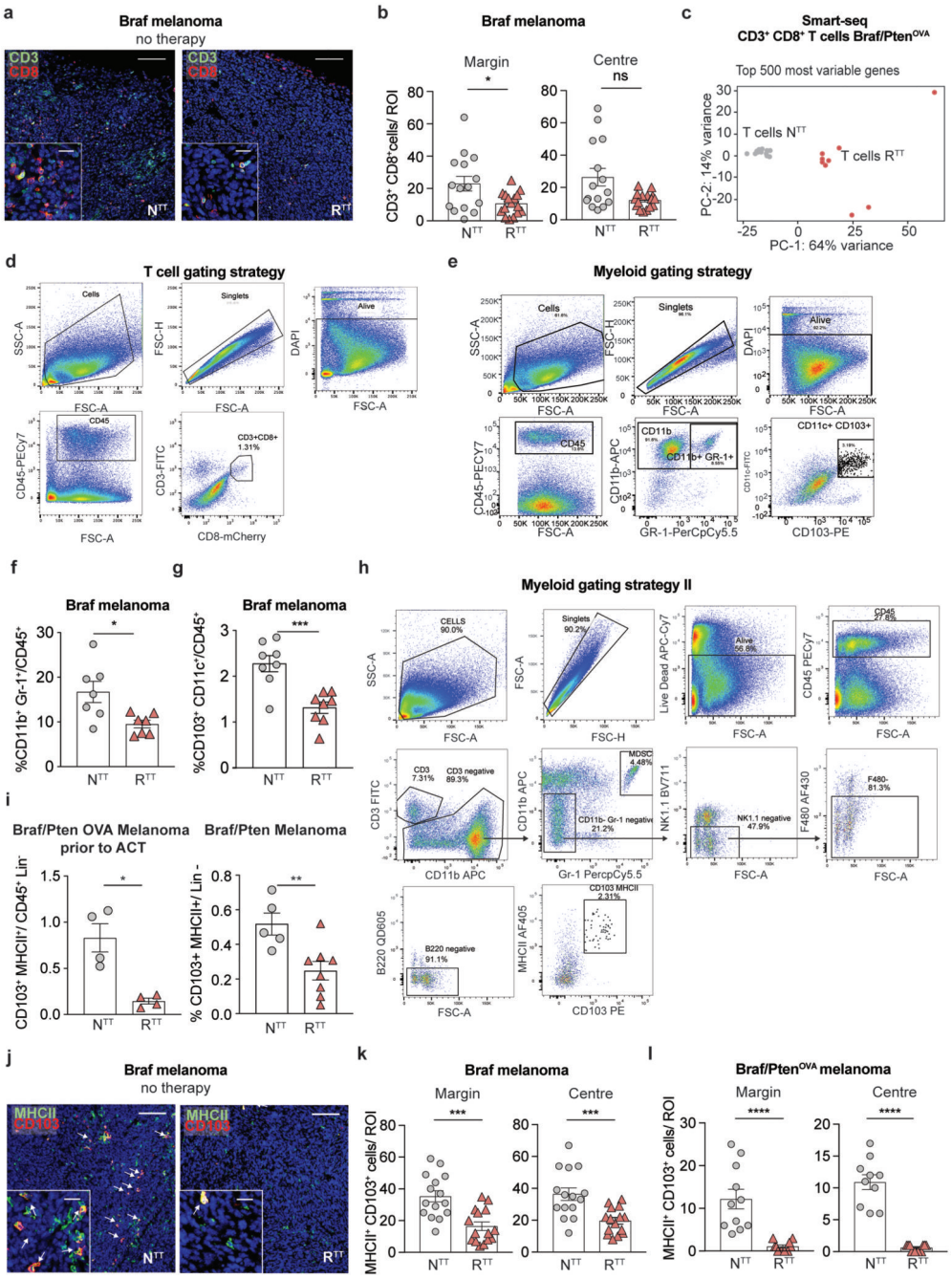


**Extended Data Fig. 4. The tumour microenvironment of $R^{TT}$ tumours is strongly remodelled.**

**a,** T cell influx into $N^{TT}$ and $R^{TT}$ Braf melanoma, assessed by IF (scale bar 100 μm and 20 μm). Experiment performed twice; representative image shown. **b,** T cell quantified separately at tumour margin and centre ($n$ = 3 tumours per condition, $N^{TT}$ $n$= 15, $R^{TT}$ $n$= 16 ROI). *P*-value: * 0.0204, ns 0.0756. **c,** PCA plot displaying top 500 most variable genes for T cells sorted from $N^{TT}$ and $R^{TT}$ Braf/$Pten^{OVA}$ tumours. **d, e** Gating strategy highlighting identification of $CD3^+$ $CD8^+$ T cells, $CD103^+$ $CD11c^+$ DCs and $CD11b^+$ $GR\text{-}1^+$ suppressive myeloid cells. **f,** Suppressive myeloid cells in Braf melanoma, assessed by flow cytometry (*n*

= 7 tumours per condition). *P*-value: * 0.023. Experiment performed 3 times; data represents pool of 2 experiments. **g,** $CD103^+$ DCs in Braf melanoma, assessed by flow cytometry (*n* = 8 tumours per condition). *P*-value: *** 0.0005. Experiment performed 3 times; data represents pool of 2 experiments. **h,** Gating strategy highlighting the identification of CD103 DCs in an alternative gating strategy (Lineage negative ($CD11b^-$,$Gr\text{-}1^-$, $NK1.1^-$, $CD3^-$, $B220^-$, $F480^-$) MHCII+ $CD103^+$ cells). **i,** Quantification of $CD103^+MHCII^+$ DCs with alternative gating strategy. (Braf/$Pten^{OVA}$ melanoma both groups, n= 4 tumours; Braf/Pten melanoma $N^{TT}$= 5 tumours, $R^{TT}$= 8 tumours). Experiment performed once. *P*-value: * 0.0185, ** 0.0083. **j, k** $CD103^+MHCII^+$ DCs in $N^{TT}$ and $R^{TT}$ Braf melanoma, assessed by IF staining in **(j)** displayed as a representative picture (scale bar 100 μm and 20 μm) (Experiment performed twice) and **(k)** quantified separately at tumour margin and centre (*n* = 3 tumours per condition, all groups 15 ROIs). *P*-value: *** 0.0002, *** 0.0010. **l,** $CD103^+MHCII^+$ DCs in $N^{TT}$ and $R^{TT}$ Braf/$Pten^{OVA}$ melanoma quantified separately at tumour margin and centre (*n* = 2 tumours per condition, all groups 10 ROI, except $N^{TT}$ margin *n* = 11). *P*-value: **** 5.7E-6, 1.1E-5. Data in **b, f, g, i, k, l** displayed as mean ± SEM and analysed by two-tailed unpaired t–test with Welch correction for unequal variance or with Mann-Whitney-U-test if not normal distributed. * $P < 0.05$, ** $P < 0.01$, *** $P < 0.001$, **** $P < 0.0001$, ns = non-significant.





Europe PMC Funders Author Manuscripts

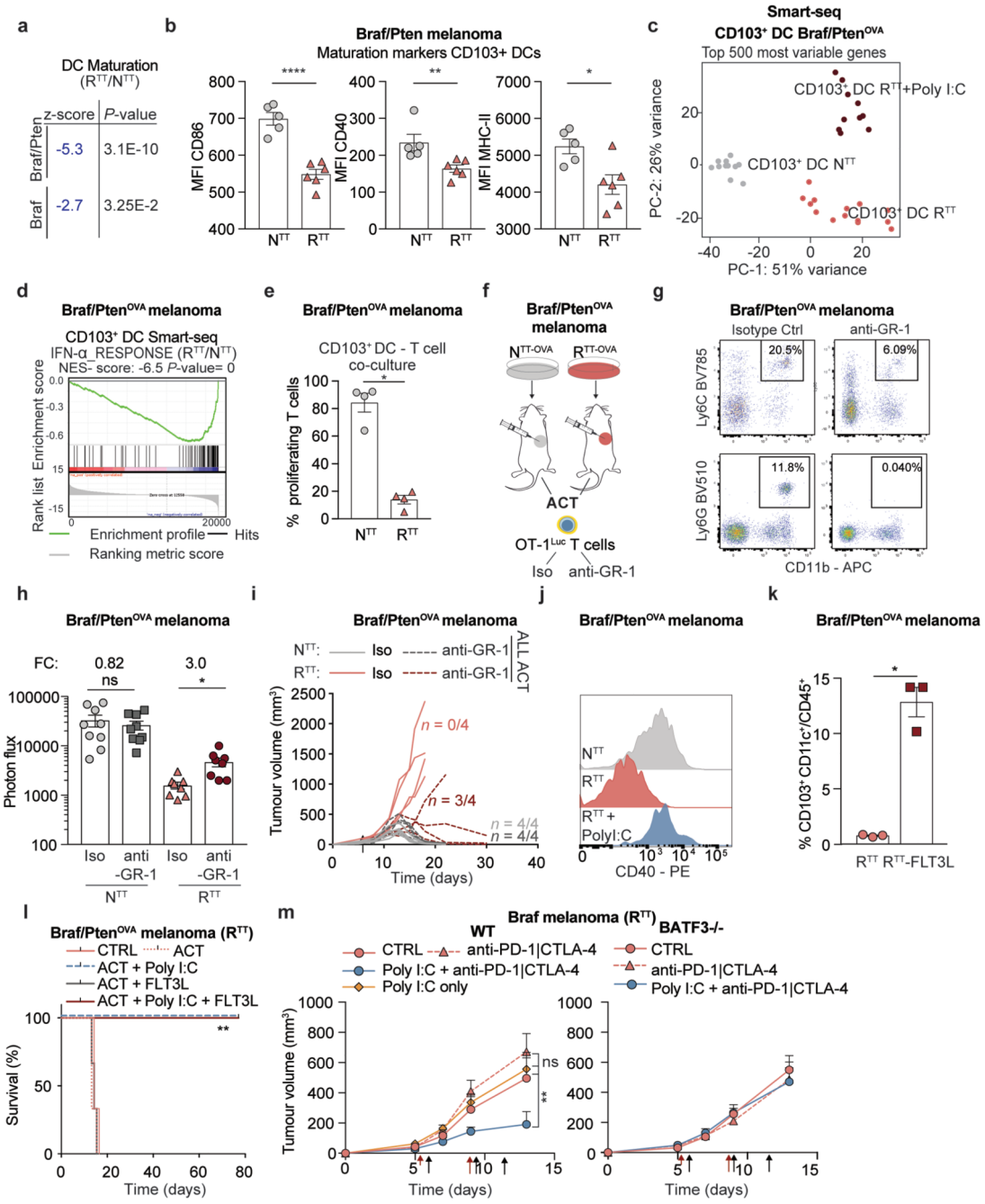


**Extended Data Fig. 5. Modulation of the myeloid cell compartment restores immunotherapy response.**

**a,** DC maturation score comparing gene expression profiles of $R^{TT}$ vs. $N^{TT}$ tumours (Braf/Pten $N^{TT}$, Braf $N^{TT}$, BRAF $R^{TT}$ $n = 3$; Braf/Pten $R^{TT}$ $n = 4$ tumours). **b,** Mean fluorescence intensity (MFI) of maturation markers on $CD103^+$ DCs from $N^{TT}$ and $R^{TT}$ Braf/Pten melanoma ($N^{TT}$, $n = 5$; $R^{TT}$, $n = 6$ tumours), assessed by flow cytometry. Experiment performed twice with independent cell lines; representative example shown. *P*-value: **** 6.9E-5, ** 0.0043, * 0.0149. **c,** PCA plot displaying top 500 most variable genes for




Europe PMC Funders Author Manuscripts

CD103$^{+}$ DCs sorted from N$^{TT}$ and R$^{TT}$ ± Poly I:C Braf/Pten$^{OVA}$ tumours. **d,** GSEA of IFN-alpha response in CD103$^{+}$ DCs sorted from R$^{TT}$ vs. N$^{TT}$ Braf/Pten$^{OVA}$ melanoma**.** **e,** Quantification of T cell proliferation based on CFSE dilution in DC co-culture assays displayed in Fig. 3i ($n$ = 4 tumours per condition). *P*-value: * 0.029. **f,** Scheme outlining experiment to assess impact of depleting suppressive myeloid cells on ACT in Braf/Pten$^{OVA}$ tumours. **g,** Depletion of Ly6C$^{+}$CD11b$^{+}$ and Ly6G$^{+}$CD11b$^{+}$ cells in blood 3 days post anti-GR-1 administration. **h,** Tumour infiltration of effector OT-1$^{Luc}$ T cells measured by BLI at 24h post ACT in Braf/Pten$^{OVA}$ tumour bearing mice treated with Isotype CTRL or anti-GR-1 antibody ($n$ = 9, 9, 8, 8 mice from left to right). Experiment performed 3 times; representative example shown. *P*-value: ns 0.53, * 0.0128. **i,** Treatment response of Braf/Pten$^{OVA}$ tumours treated with ACT or anti-GR-1 plus ACT (N$^{TT}$ ACT+ISO, $n$ = 6; R$^{TT}$ ACT+ISO, $n$ = 4; N$^{TT}$ ACT+anti-GR-1, $n$ = 6; R$^{TT}$ ACT+anti-GR-1, $n$ = 4 mice). **j,** DC maturation in Poly I:C injected Braf/Pten$^{OVA}$ tumours assessed by CD40 expression using flow cytometry. **k,** CD103$^{+}$ DC influx in R$^{TT}$ tumours overexpressing FLT3L, assessed by flow cytometry ($n$ = 3 tumours). *P*-value: * 0.0118. **l,** Survival in response to ACT ± Poly I:C ± FLT3L in R$^{TT}$ Braf/Pten$^{OVA}$ tumours. (R$^{TT}$ CTRL, R$^{TT}$ + ACT, R$^{TT}$ FLT3L + ACT, $n$ = 3; R$^{TT}$ + ACT + Poly I:C, R$^{TT}$ FLT3L + ACT+ Poly I:C, $n$ = 4 mice). Experiment performed twice; representative example shown. *P*-value: ** 0.0100. **m,** Treatment response of R$^{TT}$ Braf melanoma in WT mice (left) and BATF3$^{-/-}$ mice (right) treated with indicated therapies; black arrows indicate anti-PD-1/CTLA-4 administration, red arrows indicate Poly I:C injection (CTRL, anti-PD-1/CTLA-4, Poly I:C, $n$ = 6 tumours; Poly I:C + anti-PD-1/CTLA-4, $n$ = 4 tumours). Experiment performed twice; representative example shown. *P*-value: ** 0.01, ns 0.1931. Data in **b, e, h, k, m** is displayed as mean ± SEM. Data analysis **b, h, k** two-tailed unpaired t-test with Welch correction for unequal variance or with Mann-Whitney-U-test if not normal distributed **l** two-sided log-rank test (Mantel-Cox) test **m** two-way ANOVA. * $P$ < 0.05, ** $P$ < 0.01, *** $P$ < 0.001, **** $P$ < 0.0001, ns = non-significant.

Europe PMC Funders Author Manuscripts

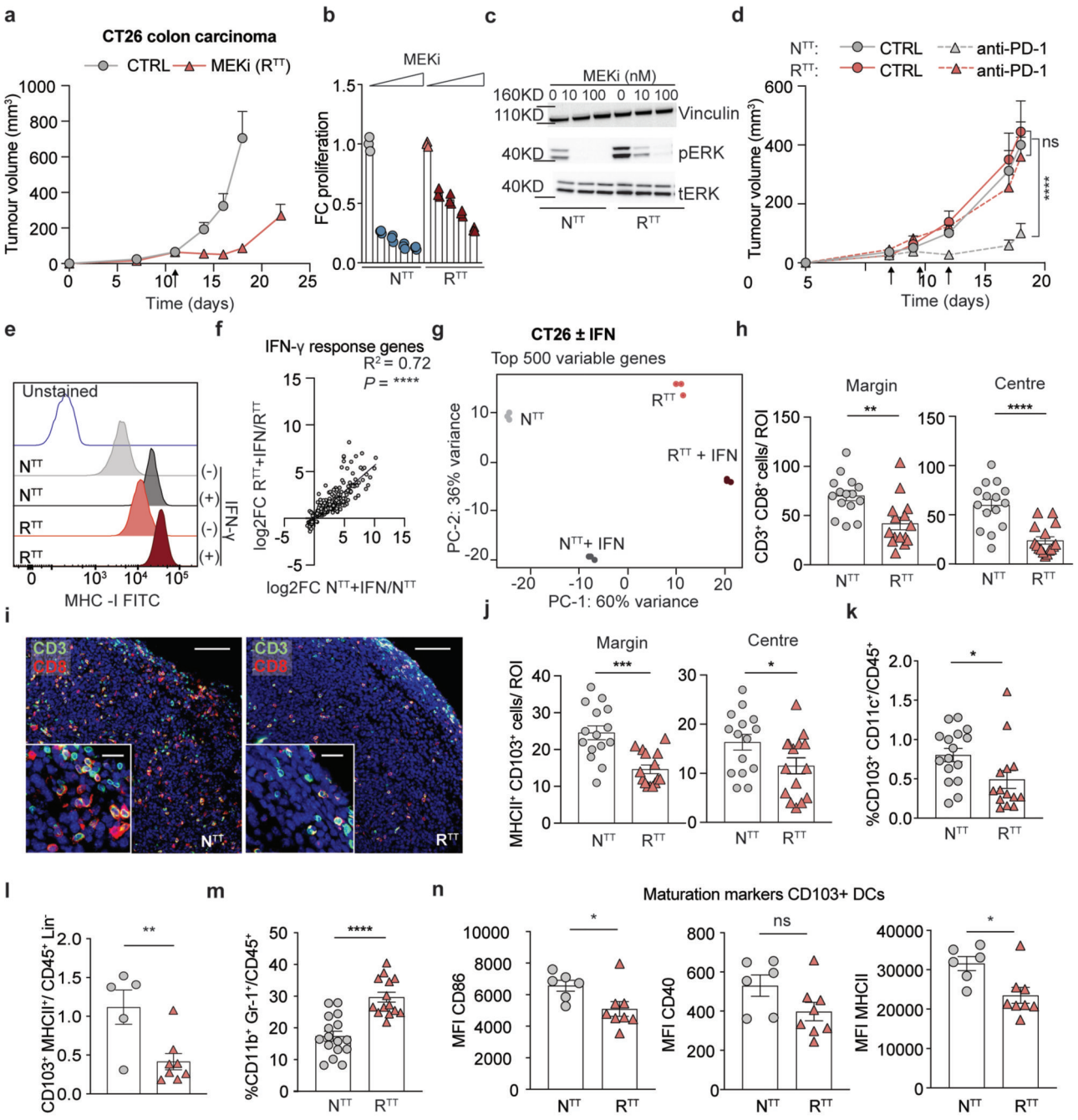


**Extended Data Fig. 6. The CT26 colon carcinoma model displays cross-resistance and an immune-evasive TME.**

**a,** Treatment response of subcutaneously injected CT26 colon carcinoma (CTRL or MEKi, $n = 8$ tumours) continuously treated with TT; arrow indicating start of therapy. Experiment performed twice; representative example shown. **b,** Proliferation FC in CT26 colon carcinoma cell lines after 72h at indicated drug conditions. Line indicating FC in proliferation of $N^{TT}$ cells on lowest drug condition ($n =$ technical triplicates) (drug concentration: DMSO CTRL, 10nM, 30nM, 100nM, 300nM MEKi). **c,** pERK status in $N^{TT}$

and $R^{TT}$ CT26 colon carcinoma cell lines, 1-hour post drug exposure. Experiment performed twice; representative example shown. **d,** Treatment response in mice bearing $N^{TT}$ and $R^{TT}$ CT26 (*Kras*$^{G12D/G12D}$ *Cdkn2a* $^{-/-}$) tumours ($N^{TT}$ and $R^{TT}$ CTRL, $n = 6$; $N^{TT}$ and $R^{TT}$ anti-PD-1, $n = 14$ tumours) treated with anti-PD-1; arrows indicate therapy administration. Experiment performed 5 times; representative example shown. *P*-value: **** 1.5E-8, ns 0.2838. **e,** MHC-I surface expression of $N^{TT}$ and $R^{TT}$ cell lines (baseline and 24h post 10 ng/ml IFN-γ exposure). Experiment performed 3 times; representative example shown**. f,** Gene expression changes in $N^{TT}$ and $R^{TT}$ CT26 colon carcinoma cell lines treated with IFN-γ. Correlation between genes deregulated in $N^{TT}$ (x-Axis) and $R^{TT}$ (y-Axis) cell lines ($P < 0.05$), dots display individual genes. *P*-value: <1E-15. **g,** PCA plot displaying top 500 most variable genes for CT26 colon carcinoma cell lines treated with IFN-γ. **h, i** T cells in untreated $N^{TT}$ and $R^{TT}$ CT26 colon carcinoma tumours assessed by IF staining and **(h)** quantified separately at tumour margin and centre ($n = 3$ tumours per condition; all 15 ROI, except $R^{TT}$ centre $n = 16$) and **(i)** displayed as a representative picture (scale bar 100 μm and 20 μm). Experiment performed twice. P-value: ** 0.0017, **** 3E-5. **j,** $CD103^+$ DCs in untreated $N^{TT}$ and $R^{TT}$ CT26 colon carcinoma tumours assessed by IF staining and quantified separately at tumour margin and centre ($n = 3$ tumours per condition, all 15 ROI). *P*-value: *** 0.0002, * 0.046. **k,** $CD103^+$ DC infiltration $N^{TT}$ and $R^{TT}$ tumours of CT26 colon carcinoma, assessed by flow cytometry ($n = 16$, 14 tumours each). Data represents pool of 2 independent experiments. *P*-value: * 0.016. **l,** $CD103^+$ DC infiltration $N^{TT}$ and $R^{TT}$ tumours of CT26 colon carcinoma, alternative gating strategy displayed in Extended Data Fig. 4h ($n = 5$, 8 tumours). *P*-value: ** 0.0081. **m,** Suppressive myeloid cell infiltration in $N^{TT}$ and $R^{TT}$ tumours of CT26 colon carcinoma, assessed by flow cytometry ($n = 16$, 14 tumours each). Data represents pool of 2 independent experiments. *P*-value: **** 7E-6. **n,** MFI of indicated maturation markers on $CD103^+$ DCs from $N^{TT}$ and $R^{TT}$ CT26 colon carcinoma ($N^{TT}$, $n = 6$; $R^{TT}$, $n = 8$ tumours) assessed by flow cytometry. *P*-value: * 0.0426, ns 0.1419, * 0.0293. Experiment performed once. Data in **b, d, h, j-n** displayed as mean ± SEM. Data analysis **d** two-way ANOVA **f** two-sided Pearson correlation **h, j-n** two-tailed unpaired t–test with Welch correction for unequal variance or with Mann-Whitney-U-test if not normal distributed. * $P < 0.05$, ** $P < 0.01$, *** $P < 0.001$, **** $P < 0.0001$, ns = non-significant.

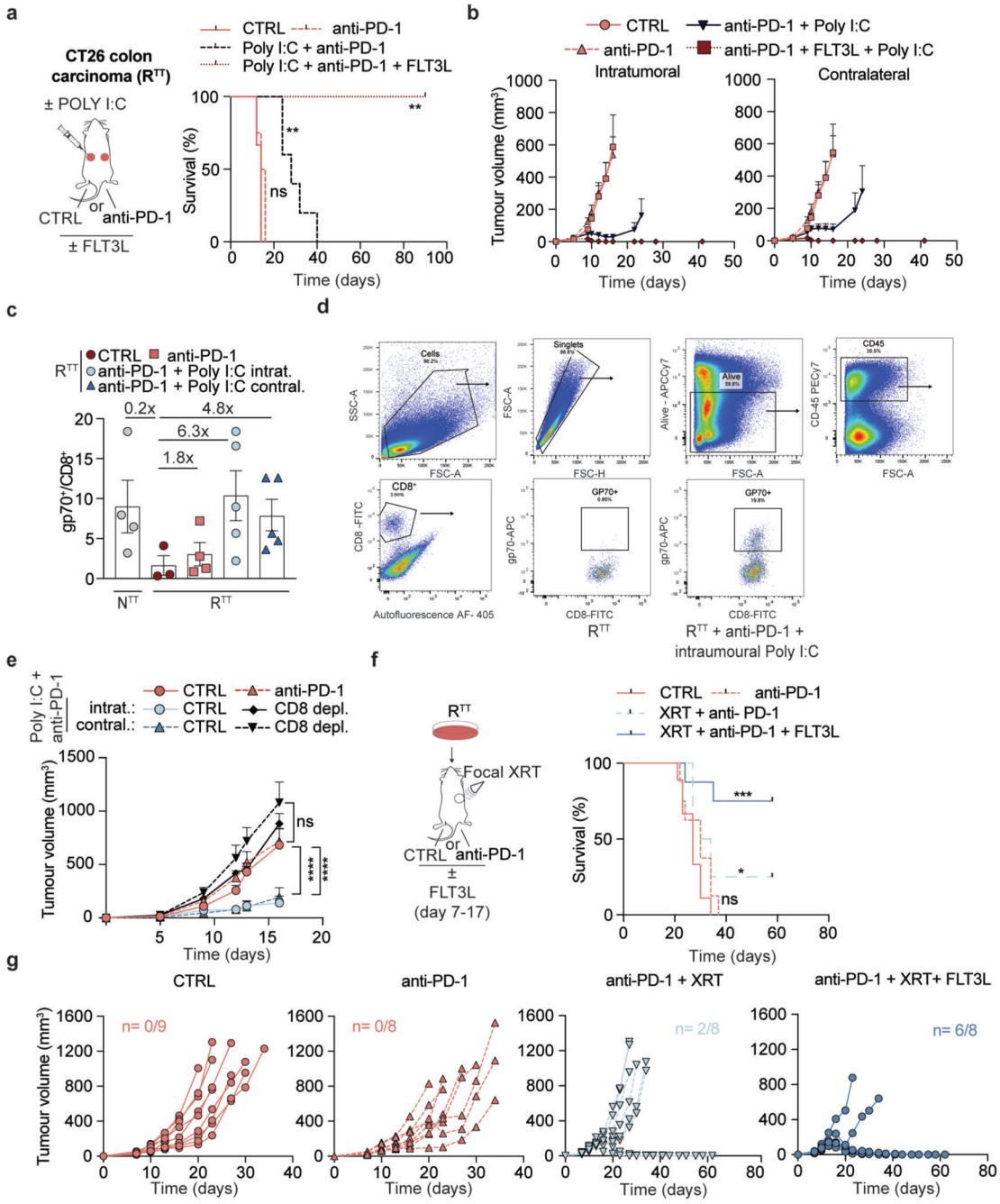


**Extended Data Fig. 7. Modulation of the CD103$^{+}$ DC compartment restores immunotherapy response in R$^{TT}$ CT26 colon carcinoma.**

**a,** Scheme outlining experiment to assess impact of maturation (intratumoural Poly I:C) and expansion (FLT3L overexpression from tumour cells) of DCs on anti-PD-1 treatment in mice bearing R$^{TT}$ CT26 colon carcinoma (left) and survival curve of mice (right, CTRL, *n* = 3; all other groups, *n* = 5 mice). Experiment performed twice; representative example shown. *P*-value: ** 0.0067. **b,** Treatment response of R$^{TT}$ CT26 colon carcinoma to anti-PD-1 (day 6, 9, 12) in combination with intratumoural Poly I:C injection (day 5, 9, 12) for




Europe PMC Funders Author Manuscripts

intratumoural (left) or contralateral tumour. (CTRL, $n = 8$, anti-PD-1 $n = 10$; contralateral and intratumoural, $n = 5$ tumours each). **c,** Influx of H2-$L^D$ MuLV gp70 specific T cells into $N^{TT}$ and $R^{TT}$ CT26 colon carcinoma treated with anti-PD-1 and Poly I:C (injected and contralateral tumour displayed separately) ($N^{TT}$ CTRL, $n = 4$; $R^{TT}$ CTRL, $n = 3$; $R^{TT}$ anti-PD-1, $n = 4$; anti-PD-1 + Poly I:C intratumoural, anti-PD-1 + Poly I:C contralateral, $n = 5$ tumours). Experiment performed once. *P*-value: all ns. **d,** Gating strategy highlighting the identification of gp70 Tetramer positive T cells. **e,** Treatment response to anti-PD-1 (day 6, 9, 12) in combination with intratumoural Poly I:C injection (day 5, 9, 12) ± CD8 depletion (day 3, 5, 10, 14), injected and contralateral tumour displayed separately. (CTRL, anti PD-1, anti-PD-1 + Poly I:C + CD8 depletion $n = 6$; anti-PD-1 + Poly I:C, $n = 7$ mice). Experiment performed once. *P*-value: ******** 1.9E-6, ****2.5 E-5, ns 0.9989. **f,** Scheme outlining experiment to assess impact of focal radiation ± anti-PD-1 ± FLTL3L in mice bearing $R^{TT}$ CT26 colon carcinoma (left) and survival curve of mice treated with indicated therapies (CTRL, $n = 9$; anti-PD-1, $n = 8$; XRT + anti-PD-1, $n = 8$; XRT + anti-PD-1 + FLT3L, $n = 8$ mice). Experiment performed once. *P*-value: ******* 0.0006, ** 0.0389. **g,** Treatment response of $R^{TT}$ CT26 colon carcinoma to anti-PD-1 (day 15, 18, 21, 24) in combination with focal radiation (9 Gy, day 14) and FLT3L administration (10 consecutive doses, initiated on day 7). Number of responding mice indicated in graph. Data in **b, c, e** displayed as mean ± SEM. Data analysis **a, f** two-sided log rank (Mantel-Cox) test **e** two-way ANOVA. * $P < 0.05$, ** $P < 0.01$, *** $P < 0.001$, **** $P < 0.0001$, ns = non-significant.

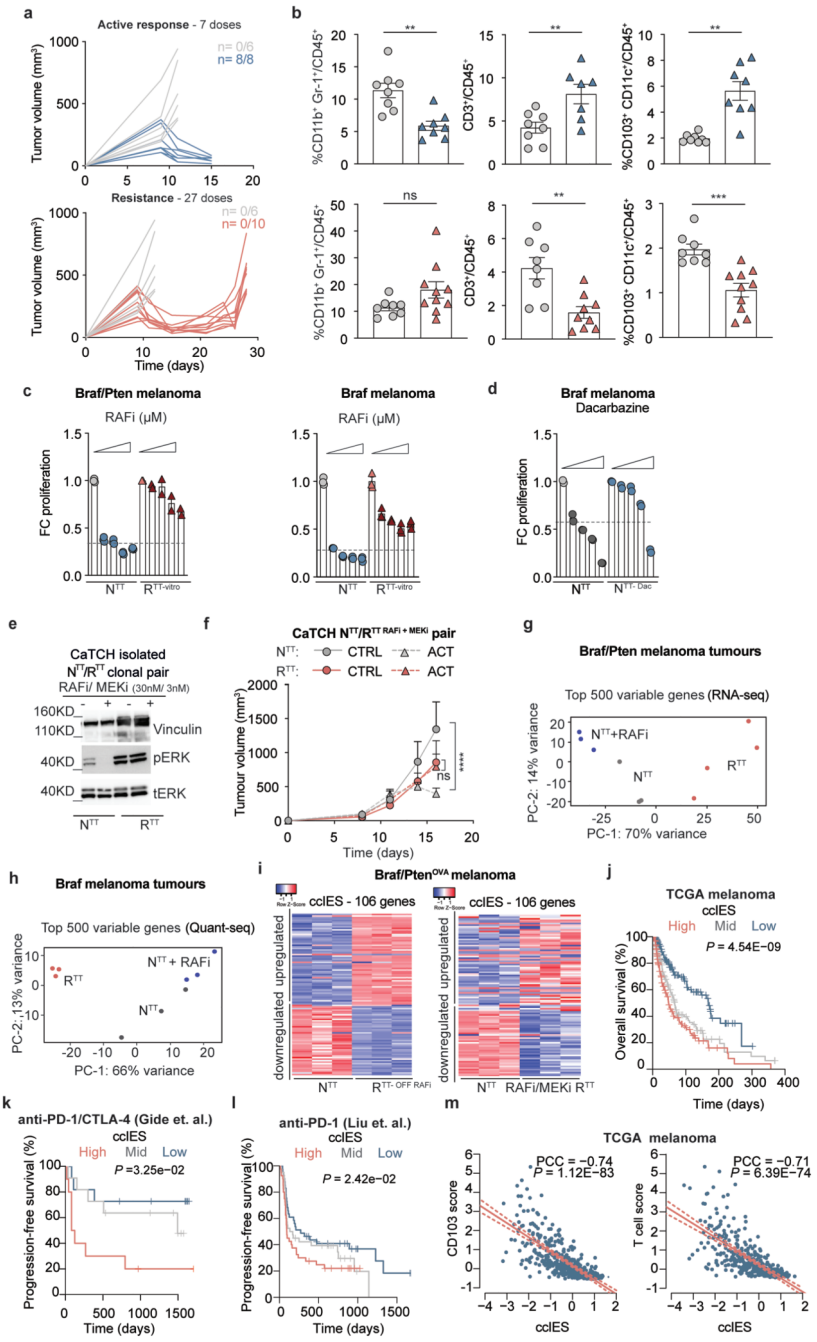


**Extended Data Fig. 8. Cross-resistance to immunotherapy is cell intrinsic, acquired during resistance formation and specific to MAPK pathway inhibition.**

**a,** Active response to RAFi in $N^{TT}$ Braf/Pten tumours (7 doses) and resistance formation upon 27 doses (CTRL, $n = 6$; 7 doses $n = 8$, 27 doses $n = 10$ tumours). **b,** Characterization of suppressive myeloid cells, T cells and $CD103^{+}$DCs in Braf/Pten tumours actively responding to RAFi (7 doses) and in relapsing tumours, fully resistant to RAFi (27 doses) ($n = 8$ tumours per group; except $CD3^{+}$ 7 doses, $n = 7$; $CD3^{+}$ 27 doses, $n = 9$; $CD11b^{+}$ Gr-1, $CD103^{+}$ 27 doses, $n = 10$). Experiment performed twice; representative example shown.

*P*-value top row: ** 0.0011, ** 0.0085, ** 0.0014; bottom row: ns 0.08, ** 0.0018, *** 0.0003. **c,** Proliferation FC in Braf/Pten and Braf melanoma cell lines (made resistant to TT *in vitro*) after 72h at indicated drug conditions. Line indicating FC in proliferation of $N^{TT}$ cells on lowest drug condition (*n* = technical triplicates), (drug concentration: DMSO CTRL, 100nM, 300nM, 1μM, 3μM RAFi). **d,** Proliferation FC of Braf melanoma cell lines after 72h in indicated drug conditions of $N^{TT}$ and $N^{TT\text{-}Dacarbazine}$ cell lines (*n* = technical duplicates), (drug concentration: CTRL, 10 μg, 50 μg, 100 μg, 500 μg Dacarbazine). **e,** pERK status in CaTCH-isolated $N^{TT}$ and $R^{TT}$ Braf/Pten cell lines, 1-hour post drug exposure. Experiment performed twice; representative example shown. **f,** Treatment response to ACT in matched CaTCH isolated $N^{TT}$ and $R^{TT}$ Braf/$Pten^{OVA}$ tumours (CTRL, *n* = 3 mice, ACT, *n* = 5 mice). Experiment performed twice; representative example shown. *P*-value: **** 3E-5, ns 0.9871. **g, h** PCA plot displaying top 500 most variable genes for (**g**) Braf/Pten and (**h**) Braf melanoma tumours. **i,** Expression of genes comprising the ccIES in sorted $N^{TT}$ and $R^{TT}$ Braf/$Pten^{OVA}$ melanoma cells (left, tumours were not exposed to RAFi) (all groups *n* = 3 tumours) and in sorted RAFi/MEKi $R^{TT}$ melanoma cells (all groups *n* = 3 tumours) (right). **j,** Overall survival stratified based on ccIES expression in TCGA melanoma patients (*n* = 469 patients). **k, l** Progression-free survival stratified based on ccIES expression in patients receiving **(k)** anti-PD-1/CTLA-4 combination therapy (*n* = 32 patients) or **(l)** anti-PD-1 monotherapy (*n* = 121 patients). **m,** Correlation of ccIES with CD103 score and T cell score in TCGA melanoma patients (*n* = 469 patients). Data in **a, b, c, d, f,** displayed as mean ± SEM. Data analysis **b** two-tailed unpaired t–test with Welch correction for unequal variance or with Mann-Whitney-U-test if not normal distributed **f** two-way ANOVA. *P*-value in **j-l** derived from a Cox proportional hazards model using gene score as a continuous variable and analysis in **m** two-sided Pearson Correlation coefficient (PCC). * $P < 0.05$, ** $P < 0.01$, *** $P < 0.001$, **** $P < 0.0001$, ns = non-significant.

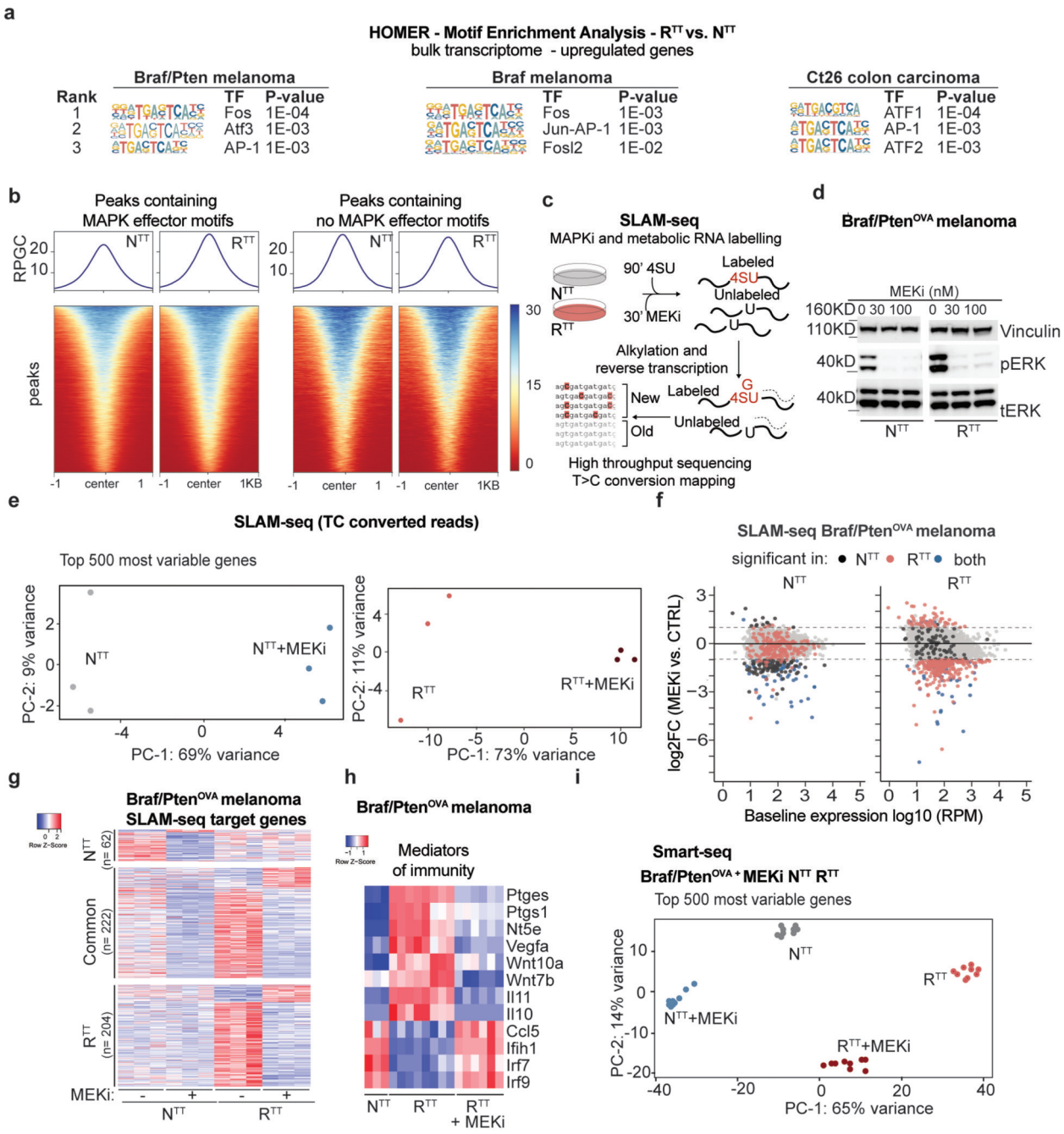


**Extended Data Fig. 9. The reactivated MAPK pathway in $R^{TT}$ tumours has a qualitatively and quantitatively different output.**

**a,** HOMER motif enrichment analysis of upregulated genes comparing $R^{TT}$ vs. $N^{TT}$ tumours of indicated models. **b,** Heatmap of normalized (RPGC) gene accessibility tracks. Depicted are accessibility profiles for peaks containing motifs of MAPK effectors (left, containing any of the following motifs: AP-1, Fosl2, Fra1, Fra2, Jun-AP-1, c-Jun-CRE, JunB, JunD, ATF2, ATF3) or peaks without MAPK motifs (right). **c,** Scheme illustrating workflow of SLAM-seq experiment in $N^{TT}$ and $R^{TT}$ (RAFi resistant) Braf/Pten$^{OVA}$ melanoma. **d,** pERK




Europe PMC Funders Author Manuscripts

Europe PMC Funders Author Manuscripts

status in $N^{TT}$ and $R^{TT}$ Braf/$Pten^{OVA}$ melanoma, 1-hour post exposure to MEKi. Experiment performed twice; representative example shown. **e,** PCA Plot highlighting the Top 500 most variable genes (based on reads containing TC conversions) in SLAM-seq dataset. **f,** Changes in abundance of newly synthesized mRNA (detected in SLAM-seq based on T>C conversions) in $N^{TT}$ (left) or $R^{TT}$ (right) Braf/$Pten^{OVA}$ melanoma treated with MEKi for 2 hours. Significant targets genes identified in SLAM-seq in $N^{TT}$ cells (black), $R^{TT}$ cells (red) or both (blue) are labelled. Only genes with >2RPMu in CTRL or MEKi conditions displayed. **g,** Expression of newly synthesized mRNA (RPMu) of 488 target genes identified with SLAM-seq (log2FC<−1, >1, padj<0.1, >2 RPMu) in $N^{TT}$ and $R^{TT}$ Braf/$Pten^{OVA}$ melanoma ± MEKi. Target genes are grouped according to their expression change upon MEKi in both cell lines. ($N^{TT}$: genes that change expression upon MEKi only in $N^{TT}$ cell line ($R^{TT}$ FC <1.5), $R^{TT}$: genes that change expression upon MEKi only in $R^{TT}$ cell line ($R^{TT}$ FC <1.5), Common: gene expression FC upon MEKi exceeds ±1.5 in both cell lines). **h,** Expression of selected immune-related genes in $N^{TT}$, $R^{TT}$ and $R^{TT}$ + MEKi (72h) sorted Braf/$Pten^{OVA}$ melanoma cells from Rag2-/-mice ($N^{TT}$, $n = 3$ $R^{TT}$, $n = 8$; $R^{TT}$+ MEKi $n =$ 6 tumours). **i,** PCA plot displaying top 500 most variable genes for Braf/$Pten^{OVA}$ melanoma cells sorted from $N^{TT}$ and $R^{TT}$ tumours after 72h of MEKi or CTRL treatment.

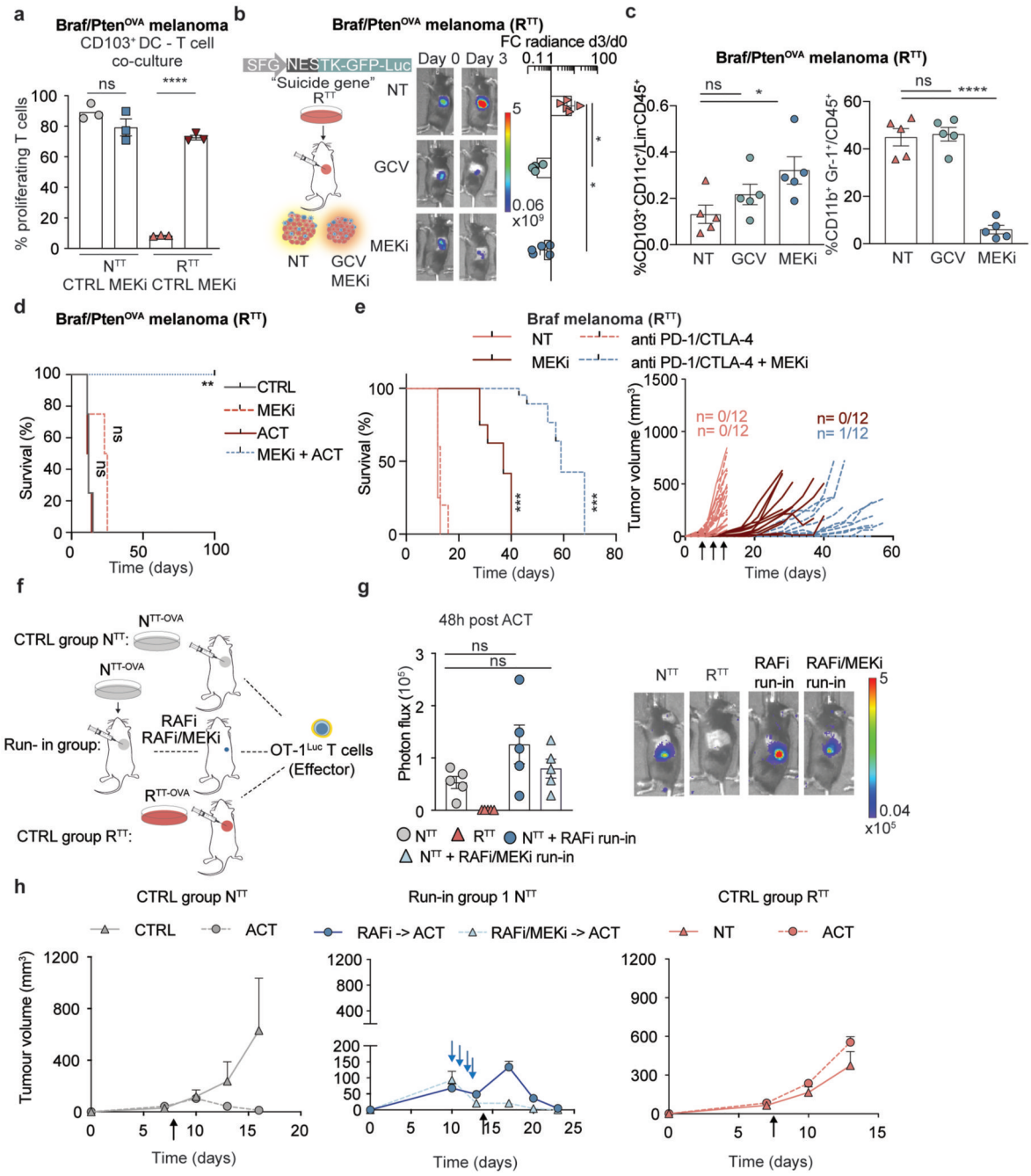


**Extended Data Fig. 10. Inhibition of the reactivated MAPK pathway in RAFi resistant $R^{TT}$ tumours restores immunotherapy response.**

**a,** Quantification of T cell proliferation based on CFSE dilution in DC co-culture assays displayed in Fig. 7f ($n$ = 3 tumours per condition). Experiment performed once. *P*-value: ns 0.21, **** 3E-5**. b,** Scheme illustrating the use of the "thymidinekinase" (HSV-TK) suicide gene (activated by ganciclovir [GCV]) to induce apoptosis in the $R^{TT}$ Braf/$Pten^{OVA}$ cancer cell line (left) and BLI image and quantification of $TGL^{+}$ $R^{TT}$ Braf/$Pten^{OVA}$ cancer cells at day 0 and 3 post GCV/MEKi administration ($n$= 5 mice) (right). Experiment

performed twice; representative example shown. *P*-value: * 0.0188, * 0.0154. **c,** $CD103^+$ DCs (left) and suppressive myeloid cells (right) in $R^{TT}$ Braf/$Pten^{OVA}$ tumours in response to GCV or MEKi administration (all groups, $n = 5$ tumours), assessed by flow cytometry. Experiment performed twice; representative example shown. *P*-value: ns 0.3766, * 0.0303, ns; ns 0.9350, **** <E−15. **d,** Survival curve illustrating treatment response in $R^{TT}$ Braf/$Pten^{OVA}$ tumour bearing mice treated with indicated therapies (all groups $n = 4$; except MEKi + ACT, $n = 5$ mice). Experiment performed twice; representative example shown. *P*-value: ** 0.0029. **e,** Survival curve and corresponding spider plot illustrating treatment response in $R^{TT}$ Braf tumour bearing mice treated with indicated therapies ($n = 6$ mice per group, 2 tumours each). Black arrows indicate immunotherapy administration, continuous MEKi was initiated on Day 5. Experiment performed twice; representative example shown. *P*-Value: *** 0.0005. **f,** Scheme illustrating experiments where mice bearing established $N^{TT}$ Braf/$Pten^{OVA}$ tumours were treated with a short run-in phase (4 doses) of RAFi or RAFi/MEKi and subsequently switched to ACT. **g,** Tumour infiltration of effector OT-$1^{Luc}$ T cells measured by BLI at 48h post ACT in Braf/$Pten^{OVA}$ tumour bearing mice ($n = 5$ mice per group). Experiment performed once with two independent clones. Data represents one representative clone. *P*-value: ns 0.07, 0.071. **h,** Treatment response of Braf/$Pten^{OVA}$ tumours to ACT (all groups: CTRL $n = 3$ mice, ACT $n = 5$ mice per group). Data in **a -c, g, h** displayed as mean ± SEM. Data analysis **a** two-tailed unpaired t-test **b, c** one-way ANOVA **d, e** two-sided log-rank (Mantel-Cox) test. * $P < 0.05$, ** $P < 0.01$, *** $P < 0.001$, **** $P < 0.0001$, ns = non-significant.

## Supplementary Material

Refer to Web version on PubMed Central for supplementary material.

## Acknowledgements

The authors thank the members of the Obenauf laboratory and Zuber laboratory (IMP) for discussions; S. Rieser and M. Aichinger (IMP) for plasmid templates, the parental CT26 cell line, Lenti-X cells and mouse lines; Eva Crespo-Rodriguez (ICR London) for support with set-up of XRT experiments; J. Moon (Univ. Michigan) for providing OT-1 Luc Thy1.1 mice; M. Bosenberg for providing the parental ($N^{TT}$) Braf and Braf/Pten cell lines; T. Burkhard and Kimon Froussios for NGS analysis; P. Garin-Chesa, A. Pauli, F. Holstein and S. Cronin for proof-reading of the manuscript, L. Formenti for contributing the western blot in Extended Data Fig. 8e. This work was supported by grants from the European Research Council ("CombaTCancer" #759590; A.O.) and the Viennese Science and Technology Fund (#LS-16-063; A.O. & T.W.). S.V. is supported by the Medical Research Council (MC_UU_12022/7). This work was also supported by a National Health and Medical Research Council of Australia (NHMRC) Program grant (R.A.S. & G.V.L.) and NHMRC Practitioner Fellowship grant (R.A.S. & G.V.L). G.V.L, R.A.S. and J.S.W. are supported by NHMRC Fellowships, G.V.L is also supported by the University of Sydney Medical Foundation and Melanoma Institute Australia. Support from the Ainsworth Foundation and colleagues at Melanoma Institute Australia, Mater Hospital, the Royal Prince Alfred Hospital, Royal North Shore Hospital, Westmead Hospital and New South Wales Health Pathology are also gratefully acknowledged.

## Data availability

Gene expression data (RNA-seq, Quant-seq, SMART-seq and SLAM-seq) and ATAC-seq data that support the findings of this study have been deposited in the Gene Expression Omnibus (GEO) under accession codes GSE132443. The human melanoma transcriptomic data was derived from the TCGA Network (loaded from cBio portal, July 2019). Gene expression data for patients receiving checkpoint blockade is available from Gide et al.

(PRJEB23709) and Liu et al. (dbGAP phs000452.v3.p1)[43,44]. Source data for Extended Data Fig. 2b, 2e, 6c, 8e, 9d have been provided as Source Data files. All other data supporting the findings of this study are available from the corresponding author on reasonable request.

## References


1. Luke J, Flaherty K, Ribas A, et al. Targeted agents and immunotherapies: optimizing outcomes in melanoma. Nat Rev Clin Oncol. 2017; 14: 463–482. [PubMed: 28374786]
2. Pavlick AC, Fecher L, Ascierto PA, Sullivan RJ. Frontline Therapy for BRAF-Mutated Metastatic Melanoma: How Do You Choose, and Is There One Correct Answer? American Society of Clinical Oncology Educational Book. 2019. 564–571. [PubMed: 31099689]
3. Robert C, et al. Five-Year Outcomes with Dabrafenib plus Trametinib in Metastatic Melanoma. N Engl J Med. 2019; 381: 626–636. [PubMed: 31166680]
4. Larkin J, et al. Five-Year Survival with Combined Nivolumab and Ipilimumab in Advanced Melanoma. N Engl J Med. 2019; 381: 1535–1546. [PubMed: 31562797]
5. Seth R, et al. Systemic Therapy for Melanoma: ASCO Guideline. J Clin Oncol. 2020; 38: 3947–3970. [PubMed: 32228358]
6. Michielin O, et al. Cutaneous melanoma: ESMO Clinical Practice Guidelines for diagnosis, treatment and follow-up. Annals of Oncology. 2019; 30: 1884–1901. [PubMed: 31566661]
7. Ackerman A, et al. Outcomes of patients with metastatic melanoma treated with immunotherapy prior to or after BRAF inhibitors. Cancer. 2014; 120: 1695–1701. [PubMed: 24577748]
8. Johnson DB, Sullivan RJ. Sequencing Treatment in BRAFV600E mutant melanoma: Anti PD-1 before and after BRAF inhibitioN. Journal of Immunotherapy. 2017. 1–5. [PubMed: 27828929]
9. Tétu P, et al. Benefit of the nivolumab and ipilimumab combination in pretreated advanced melanoma. European Journal of Cancer. 2018; 93: 147–149. [PubMed: 29449059]
10. Mason R, et al. Combined ipilimumab and nivolumab first-line and after BRAF-targeted therapy in advanced melanoma. Pigment Cell Melanoma Res. 2019; 33: 358–365. [PubMed: 31587511]
11. Frederick DT, et al. BRAF inhibition is associated with enhanced melanoma antigen expression and a more favorable tumor microenvironment in patients with metastatic melanoma. Clinical Cancer Research. 2013; 19: 1225–1231. [PubMed: 23307859]
12. Cooper ZA, et al. Distinct clinical patterns and immune infiltrates are observed at time of progression on targeted therapy versus immune checkpoint blockade for melanoma. OncoImmunology. 2016; 5: 1–8.
13. Hugo W, et al. Non-genomic and Immune Evolution of Melanoma Acquiring MAPKi Resistance. Cell. 2015; 162: 1271–1285. [PubMed: 26359985]
14. Hugo W, et al. Genomic and Transcriptomic Features of Response to Anti-PD-1 Therapy in Metastatic Melanoma. Cell. 2016; 165: 35–44. [PubMed: 26997480]
15. Steinberg SM, et al. Myeloid Cells That Impair Immunotherapy Are Restored in Melanomas with Acquired Resistance to BRAF Inhibitors. Cancer Research. 2017; 77: 1599–1610. [PubMed: 28202513]
16. Orgaz JL, et al. Myosin II Reactivation and Cytoskeletal Remodeling as a Hallmark and a Vulnerability in Melanoma Therapy Resistance. Cancer Cell. 2020; 37: 85–103. e9 [PubMed: 31935375]
17. Welsh SJ, Rizos H, Scolyer RA, Long GV. Resistance to combination BRAF and MEK inhibition in metastatic melanoma: Where to next? European Journal of Cancer. 2016; 62: 76–85. [PubMed: 27232329]
18. Peng W, et al. Loss of PTEN Promotes Resistance to T Cell-Mediated Immunotherapy. Cancer Discovery. 2016; 6: 202–216. [PubMed: 26645196]
19. Salmon H, et al. Expansion and Activation of CD103+ Dendritic Cell Progenitors at the Tumor Site Enhances Tumor Responses to Therapeutic PD-L1 and BRAF InhibitioN. Immunity. 2016; 44: 924–938. [PubMed: 27096321]






Europe PMC Funders Author Manuscripts

20. Umkehrer C, et al. Isolating live cell clones from barcoded populations using CRISPRa-inducible reporters. Nature Biotechnology. 2020; 1–23. DOI: 10.1038/s41587-020-0614-0
21. Ebert PJR, et al. MAP Kinase Inhibition Promotes T Cell and Anti-tumor Activity in Combination with PD-L1 Checkpoint Blockade. Immunity. 2016; 44: 609–621. [PubMed: 26944201]
22. Callahan MK, et al. Paradoxical Activation of T Cells via Augmented ERK Signaling Mediated by a RAF Inhibitor. Cancer Immunology Research. 2014; 2: 70–79. [PubMed: 24416731]
23. Sharma P, Allison JP. The future of immune checkpoint therapy. Science. 2015; 348: 56–61. [PubMed: 25838373]
24. Sharma P, Hu-Lieskovan S, Wargo JA, Ribas A. Primary, Adaptive, and Acquired Resistance to Cancer Immunotherapy. Cell. 2017; 168: 707–723. [PubMed: 28187290]
25. Kalbasi A, Ribas A. Tumour-intrinsic resistance to immune checkpoint blockade. Nat Rev Immunol. 2020; 20: 25–39. [PubMed: 31570880]
26. Galon J, Bruni D. Approaches to treat immune hot, altered and cold tumours with combination immunotherapies. Nat Rev Drug Discov. 2019; 18: 197–218. [PubMed: 30610226]
27. Chen DS, Mellman I. Elements of cancer immunity and the cancer-immune set point. Nature. 2017; 541: 321–330. [PubMed: 28102259]
28. Spranger S, Dai D, Horton B, Gajewski TF. Tumor-Residing Batf3 Dendritic Cells Are Required for Effector T Cell Trafficking and Adoptive T Cell Therapy. Cancer Cell. 2017; 31: 711–723. e4 [PubMed: 28486109]
29. Broz ML, et al. Dissecting the Tumor Myeloid Compartment Reveals Rare Activating Antigen-Presenting Cells Critical for T Cell Immunity. Cancer Cell. 2014; 26: 638–652. [PubMed: 25446897]
30. Böttcher J, PSousa CRE. The Role of Type 1 Conventional Dendritic Cells in Cancer Immunity. TRENDS in CANCER. 2018; 4: 784–792. [PubMed: 30352680]
31. Huysamen C, Willment JA, Dennehy KM, Brown GD. CLEC9A is a novel activation C-type lectin-like receptor expressed on BDCA3+ dendritic cells and a subset of monocytes. Journal of Biological Chemistry. 2008; 283: 16693–16701. [PubMed: 18408006]
32. Garris CS, et al. Successful Anti-PD-1 Cancer Immunotherapy Requires T Cell-Dendritic Cell Crosstalk Involving the Cytokines IFN-γ and IL-12. Immunity. 2018; 49: 1148–1161. e7 [PubMed: 30552023]
33. Joyce JA, Fearon DF. T cell exclusion,immune privilege, and the tumor microenvironment. Science. 2015; 348: 69–74. [PubMed: 25838375]
34. Zelenay S, et al. Cyclooxygenase-Dependent Tumor Growth through Evasion of Immunity. Cell. 2015; 162: 1257–1270. [PubMed: 26343581]
35. Tauriello D, Palomo-Ponce S, Stork D, et al. TGFβ drives immune evasion in genetically reconstituted colon cancer metastasis. Nature. 2018; 554: 538–543. [PubMed: 29443964]
36. Engblom C, Pfirschke C, Pittet M. The role of myeloid cells in cancer therapies. Nat Rev Cancer. 2016; 16: 447–462. [PubMed: 27339708]
37. Haas L, Obenauf AC. Allies or Enemies—The Multifaceted Role of Myeloid Cells in the Tumor Microenvironment. Front Immunol. 2019; 10: 253–11. [PubMed: 30891030]
38. Hammerich L, et al. Systemic clinical tumor regressions and potentiation of PD1 blockade with in situ vaccinatioN. Nature Medicine. 2019; 25: 1–23.
39. McLaughlin M, Patin EC, Pedersen M, et al. Inflammatory microenvironment remodelling by tumour cells after radiotherapy. Nat Rev Cancer. 2020; 20: 203–217. [PubMed: 32161398]
40. Obenauf AC, et al. Therapy-induced tumour secretomes promote resistance and tumour progressioN. Nature. 2015; 520: 368–372. [PubMed: 25807485]
41. Liu C, et al. BRAF Inhibition Increases Tumor Infiltration by T cells and Enhances the Antitumor Activity of Adoptive Immunotherapy in Mice. Clinical Cancer Research. 2013; 19: 393–403. [PubMed: 23204132]
42. Koya RC, et al. BRAF Inhibitor Vemurafenib Improves the Antitumor Activity of Adoptive Cell Immunotherapy. Cancer Research. 2012; 72: 3928–3937. [PubMed: 22693252]

43. Gide TN, et al. Distinct Immune Cell Populations Define Response to Anti-PD-1 Monotherapy and Anti-PD-1/Anti-CTLA-4 Combined Therapy. Cancer Cell. 2019; 35: 238–255. e6 [PubMed: 30753825]
44. Liu D, et al. Integrative molecular and clinical modeling of clinical outcomes to PD1 blockade in patients with metastatic melanoma. Nature Medicine. 2019; 25: 1916–1927.
45. Ott PA, Bhardwaj N. Impact of MAPK Pathway Activation in BRAF(V600) Melanoma on T Cell and Dendritic Cell FunctioN. Front Immunol. 2013; 4: 346. [PubMed: 24194739]
46. Shi H, et al. Acquired resistance and clonal evolution in melanoma during BRAF inhibitor therapy. Cancer Discovery. 2014; 4: 80–93. [PubMed: 24265155]
47. Muhar M, et al. SLAM-seq defines direct gene-regulatory functions of the BRD4-MYC axis. Science. 2018; 360: 800–805. [PubMed: 29622725]
48. Herzog VA, et al. Thiol-linked alkylation of RNA to assess expression dynamics. Nat Meth. 2017; 14: 1198–1204.
49. Spranger S, Gajewski T. Impact of oncogenic pathways on evasion of antitumour immune responses. Nat Rev Cancer. 2018; 18: 139–147. [PubMed: 29326431]
50. Diaz LA, et al. The molecular evolution of acquired resistance to targeted EGFR blockade in colorectal cancers. Nature. 2012. 1–4.
51. Gajewski TF, Higgs EF. Immunotherapy with a sting. Science. 2020; 369: 921–922. [PubMed: 32820113]
52. Wculek SK, Cueto FJ, Mujal AM, et al. Dendritic cells in cancer immunology and immunotherapy. Nat Rev Immunol. 2020; 20: 7–24. [PubMed: 31467405]
53. Long JE, et al. Therapeutic resistance and susceptibility is shaped by cooperative multi-compartment tumor adaptatioN. Cell Death & Differentiation. 2019; 41: 1–14.
54. Bar-Sagi D, Knelson EH, Sequist LV. A bright future for KRAS inhibitors. Nat Cancer. 2020; 1: 25–27. [PubMed: 35121842]
55. Meeth K, Wang JX, Micevic G, Damsky W, Bosenberg MW. The YUMM lines: a series of congenic mouse melanoma cell lines with defined genetic alterations. Pigment Cell Melanoma Res. 2016; 29: 590–597. [PubMed: 27287723]
56. Castle JC, et al. Immunomic, genomic and transcriptomic characterization of CT26 colorectal carcinoma. BMC Genomics. 2014; 15: 190. [PubMed: 24621249]
57. Minn AJ, et al. Distinct organ-specific metastatic potential of individual breast cancer cells and primary tumors. J CliN Invest. 2005; 115: 44–55. [PubMed: 15630443]
58. Ochyl LJ, Moon JJ. Whole-animal Imaging and Flow Cytometric Techniques for Analysis of Antigen-specific CD8+ T Cell Responses after Nanoparticle VaccinatioN. JoVE. 2015; 1–18. DOI: 10.3791/52771
59. Picelli S, et al. Full-length RNA-seq from single cells using Smart-seq2. Nature Protocols. 2014; 9: 171–181. [PubMed: 24385147]
60. Corces MR, et al. An improved ATAC-seq protocol reduces background and enables interrogation of frozen tissues. Nat Meth. 2017; 14: 959–962.

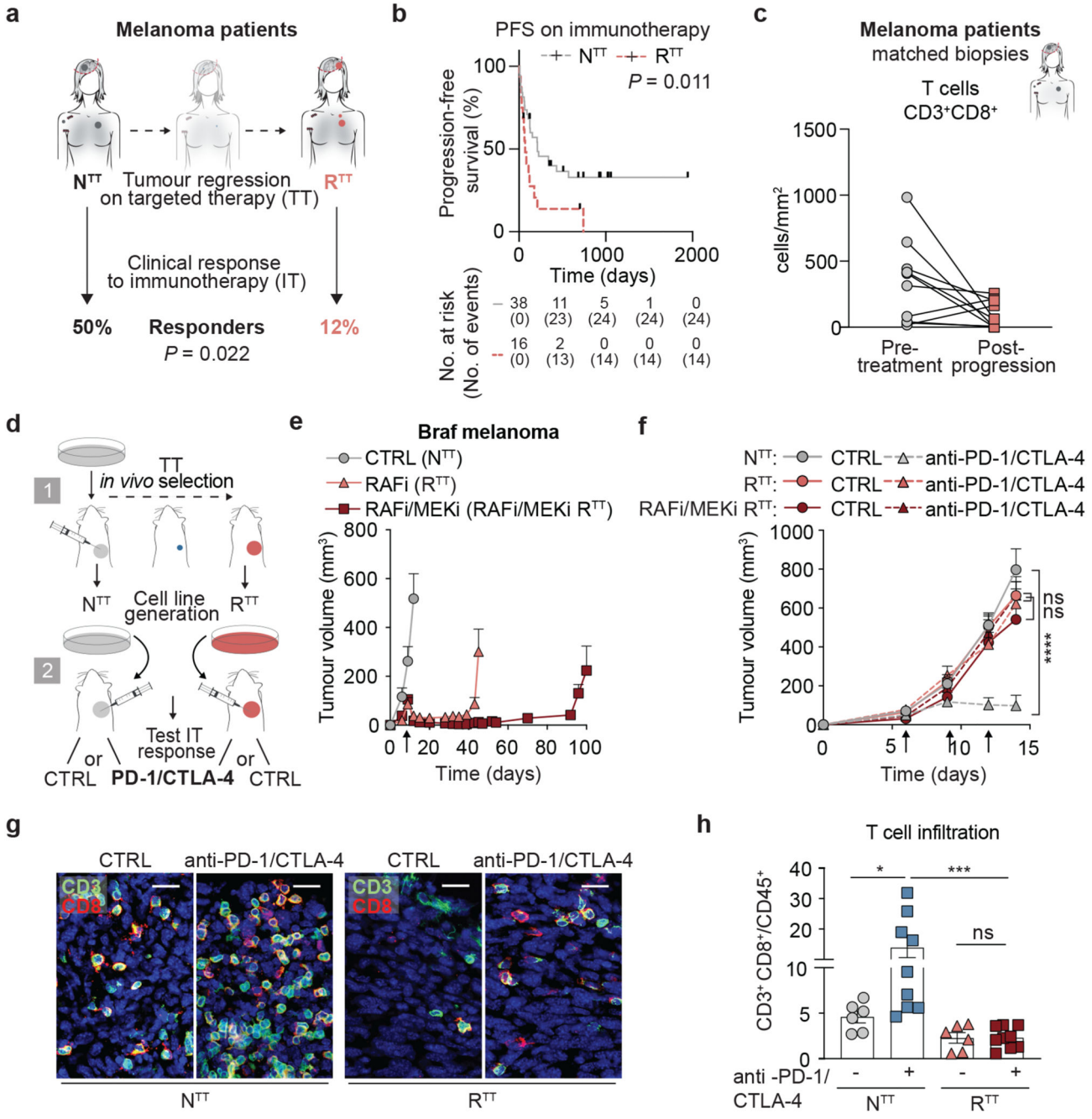


**Fig. 1. Targeted therapy resistance induces cross-resistance to immunotherapy.**

**a,** Clinical response rate and **b,** Progression-free survival (PFS) of metastatic melanoma patients in the Lausanne Patient Cohort (Supplementary Table S1) receiving immunotherapy with checkpoint inhibitors ($n$ = 54 patients). $N^{TT}$, targeted therapy (TT) naïve patients ($n$ = 38); $R^{TT}$, TT (RAFi or RAFi/MEKi) resistant patients ($n$ = 16). **c,** Quantification of T cells in tumours of $N^{TT}$ and $R^{TT}$ melanoma patients receiving MAPK pathway inhibitors (RAFi or RAFi/MEKi combination), assessed by immunofluorescence (IF) staining of matched patient biopsies ($n$ = 10 patients, Supplementary Table S2). **d,** Scheme outlining

(1) generation of $N^{TT}$ and $R^{TT}$ cell lines, before therapy or after tumour relapse on treatment and (2) testing immunotherapy response in tumours derived from $N^{TT}$ and $R^{TT}$ cell lines. **e,** Treatment response of subcutaneously injected Braf melanoma (*Braf*$^{V600E/WT}$ C*dkn2a*$^{-/-}$) tumours continuously treated with indicated TT; arrow indicating start of therapy (CTRL, $n = 6$ tumours; other groups, $n = 8$). Experiment performed 3 times; representative example shown. **f,** Treatment response in mice bearing $N^{TT}$ and $R^{TT}$ Braf melanoma; arrows indicate immunotherapy administration (all groups, $n = 8$ tumours). No targeted therapy was administered. Experiment performed 9 times; representative example shown. *P*-value: **** 4.8E-13, ns 0.9963, ns 0.7039. **g,** T cells in $N^{TT}$ and $R^{TT}$ tumours of Braf melanoma, treated with CTRL or anti-PD-1/CTLA-4 assessed by IF staining (scale bar 20 μm). Experiment performed twice; representative example shown. **h,** T cells in $N^{TT}$ and $R^{TT}$ tumours of Braf melanoma, treated with CTRL or anti-PD-1/CTLA-4 assessed by flow cytometry ($N^{TT}$ CTRL, $n = 6$; $N^{TT}$ anti-PD-1/CTLA-4, $n = 9$; $R^{TT}$ CTRL, $n = 6$; $R^{TT}$ anti-PD-1/CTLA-4, $n = 9$ tumours). Experiment performed 3 times; representative example shown. *P*-value: * 0.0196, *** 0.0009, ns >0.9999. Data in **e, f, h** displayed as mean ± standard error of mean (SEM). Data analysis **a** one-sided chi-square test **b** two-sided log-rank (Mantel-Cox) test **f** two-way ANOVA **h** one-way ANOVA. * $P < 0.05$, *** $P < 0.001$, **** $P < 0.0001$, ns = non-significant.

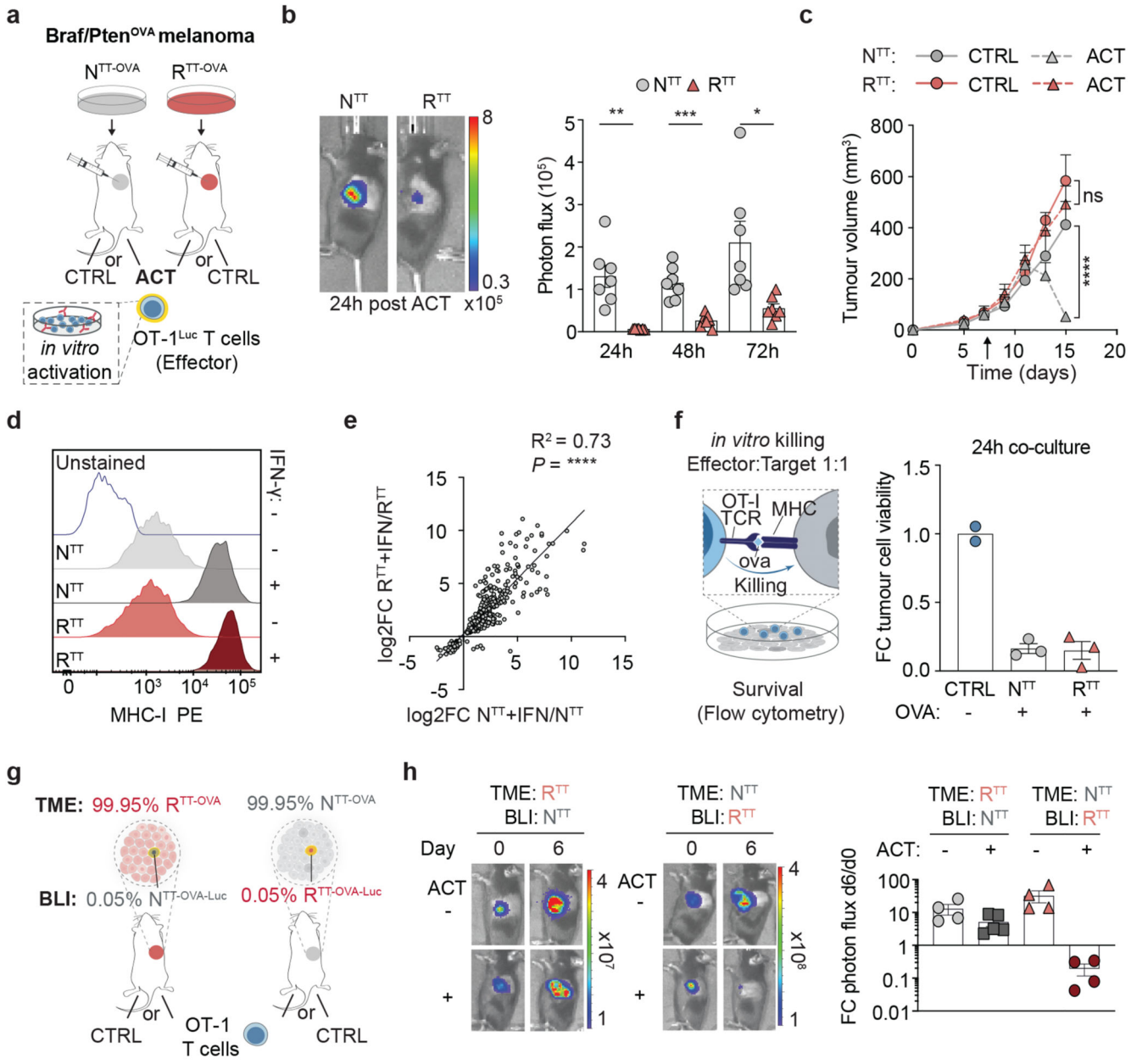


**Fig. 2. The tumour microenvironment in $R^{TT}$ tumours precludes a functional T cell response.**

**a,** Scheme outlining experiments to assess infiltration and treatment response to adoptive cell transfer (ACT) of pre-activated OT-$1^{Luc}$ effector T cells in $N^{TT}$ and $R^{TT}$ (RAFi resistant) Braf/$Pten^{OVA}$ melanoma (*$Braf^{V600E/WT}$ $Cdkn2a^{-/-}$ $Pten^{-/-}$)* tumours. **b,** Tumour infiltration of OT-$1^{Luc}$ T cells in $N^{TT}$ and $R^{TT}$ Braf/$Pten^{OVA}$ melanoma, measured by bioluminescence imaging (BLI) at indicated days (all groups, $n = 7$ tumours). Experiment performed 7 times; representative example shown. *P*-value: ** 0.0030, *** 0.0005, * 0.0210. **c,** Treatment response to ACT in Braf/$Pten^{OVA}$ tumours; arrow indicating day of ACT ($N^{TT}$, $R^{TT}$ CTRL, $n = 3$; $N^{TT}$, $R^{TT}$ ACT, $n = 5$ mice). No targeted therapy was administered. Experiment performed 7 times; representative example shown. *P*-value: ****




Europe PMC Funders Author Manuscripts

2E-6, ns 0.4934. **d,** MHC-I surface level of $N^{TT}$ and $R^{TT}$ Braf/Pten$^{OVA}$ melanoma (baseline and 24h post 10 ng/ml IFN-γ exposure). Experiment performed 3 times; representative example shown. **e,** Gene expression changes in $N^{TT}$ and $R^{TT}$ Braf/Pten$^{OVA}$ melanoma cell lines treated with IFN-γ. Correlation between genes deregulated in $N^{TT}$ (x-Axis) and $R^{TT}$ (y-Axis) cell lines ($P < 0.05$), dots display individual genes. *P*-value: <1E−15 (Supplementary Table S3). **f,** Scheme outlining the *in vitro* killing assay using pre-activated OT-1 T cells (left) and quantification of viability of Braf/Pten$^{OVA}$ melanoma cell lines after 24 h of co-culture (right) (CTRL, $n = 2$; $N^{TT\text{-}OVA}$ $R^{TT\text{-}OVA}$, $n = 3$ independent clones). **g,** Scheme outlining experiments to assess ACT response in tumours comprised of 99.95% $Luc^-$ (majority, defines the TME) and 0.05% $Luc^+$ (for BLI read-out of minority population) $N^{TT}$ or $R^{TT}$ Braf/Pten$^{OVA}$ melanoma at indicated ratios. **h,** BLI of $Luc^+$ Braf/Pten$^{OVA}$ cells at day 0 and day 6 post ACT/CTRL injection (left) and quantified fold change (FC) in BLI signal on day 6 (right) (99.95% $R^{TT}$/ 0.05% $N^{TT}$ + ACT; $n = 5$, all other groups, $n = 4$ mice). Experiment performed 3 times; representative example shown. Data in **b, c, f, h** displayed as mean ± SEM. Data analysis **b** two-tailed unpaired t-test with Welch correction for unequal variance **c** two-way ANOVA **e** two-tailed Pearson Correlation. * $P < 0.05$, ** $P < 0.01$, *** $P < 0.001$, **** $P < 0.0001$, ns = non-significant.

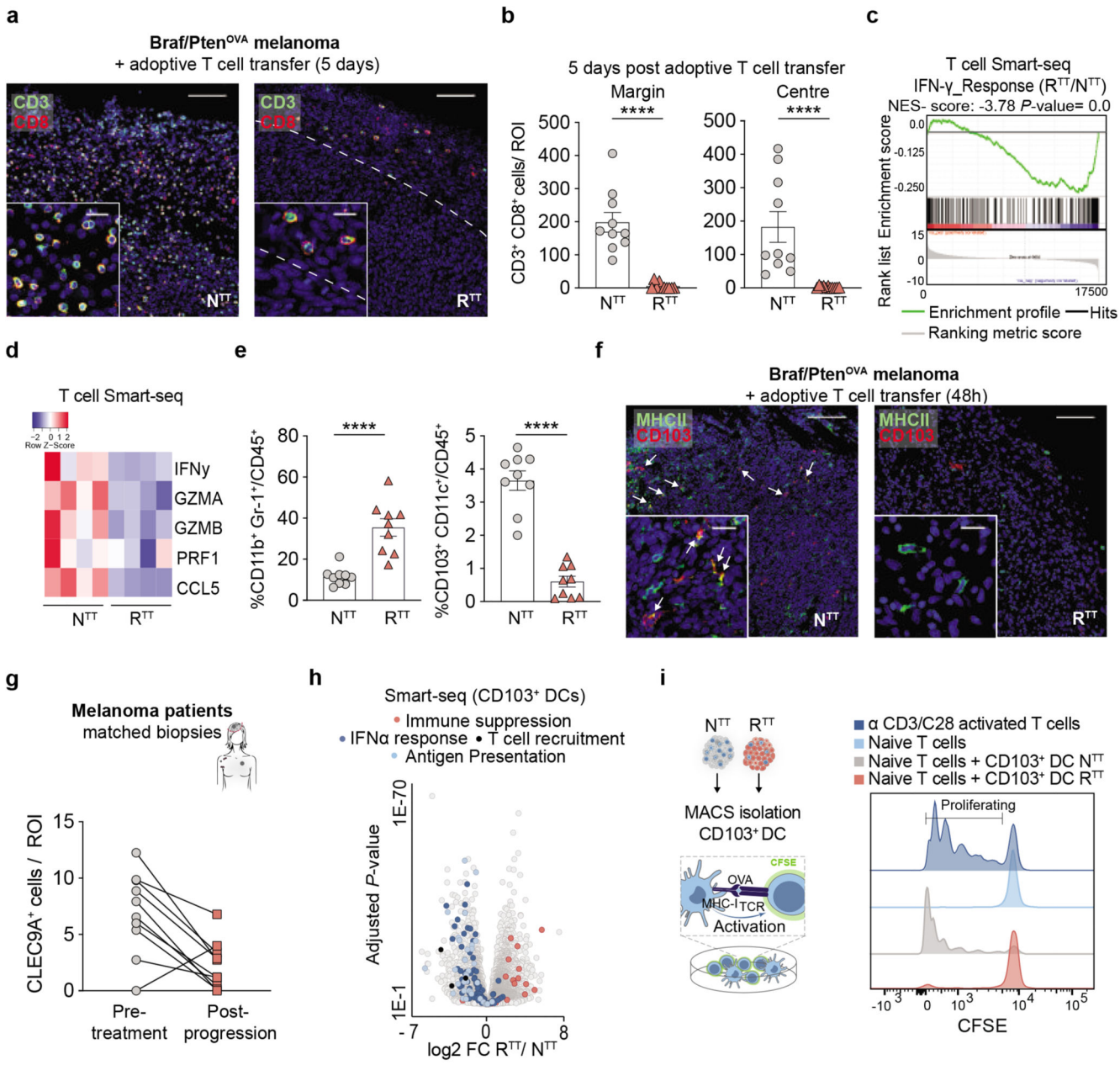


**Fig. 3. The tumour microenvironment of $R^{TT}$ tumours shows reduced and dysfunctional $CD103^+$ DCs.**

**a,** T cell influx into $N^{TT}$ and $R^{TT}$ Braf/$Pten^{OVA}$ melanoma 5 days post ACT assessed by IF (scale bar 100 μm and 20 μm). Experiment performed twice; representative image shown. **b,** T cell influx into $N^{TT}$ and $R^{TT}$ Braf/$Pten^{OVA}$ melanoma 5 days post ACT quantified separately at tumour margin and centre ($n$ = 2 tumours per condition; all groups $n$ = 10 ROI, except $R^{TT}$ centre, $n$ = 11 ROI). $P$-value: **** 1.08E-5, 5.7E-6. **c,** Gene set enrichment analysis (GSEA) of IFN-γ response in T cells sorted from $R^{TT}$ vs. $N^{TT}$ Braf/$Pten^{OVA}$ melanoma ($N^{TT}$, $R^{TT}$, $n$ = 4 tumours per condition). **d,** Heat map displaying T cell effector genes in T cells sorted from $N^{TT}$ and $R^{TT}$ tumours ($N^{TT}$, $R^{TT}$, $n$ = 4 tumours per condition).

Europe PMC Funders Author Manuscripts

**e,** Suppressive myeloid cells (left) and $CD103^+$ DCs (right) in $N^{TT}$ and $R^{TT}$ tumours of $Braf/Pten^{OVA}$ melanoma, assessed by flow cytometry ($n = 9$ tumours each). Experiment performed 5 times; displayed is a pool of 2 representative experiments. *P*-value: **** 8E-5, 9.4E-8. **f,** $CD103^+MHCII^+$ DCs in $N^{TT}$ and $R^{TT}$ $Braf/Pten^{OVA}$ melanoma, assessed by IF (scale bar 100 μm and 20 μm). Experiment performed twice; representative image shown. **g,** Quantification of $CLEC9a^+$ cells in tumours of $N^{TT}$ and $R^{TT}$ melanoma patients receiving MAPK pathway inhibitors (RAFi or RAFi/MEKi combination), assessed by IF staining of matched patient biopsies ($n = 10$ patients, Supplementary Table S2). **h,** Gene expression changes in sorted $CD103^+$ DCs from $N^{TT}$ and $R^{TT}$ $Braf/Pten^{OVA}$ melanoma assessed by Smart-seq ($N^{TT}$, $n = 4$; $R^{TT}$, $n = 5$ sorted tumours; in technical triplicates). Supplementary Table S5. **i,** Scheme outlining co-culture of $CD103^+$ DCs isolated from $N^{TT}$ and $R^{TT}$ $Braf/Pten^{OVA}$ melanoma using magnetic cell sorting (MACS) with CFSE labelled naïve OT-1 T cells to assess T cell activation potential (left) and representative histogram illustrating CFSE signal in T cells (right). Experiment performed 6 times; representative example shown. Data in **b** and **e** displayed at mean ± SEM and analysed using two-tailed unpaired t-test with Welch correction for unequal variance or Mann-Whitney U test if not normal distributed. **** $P < 0.0001$.

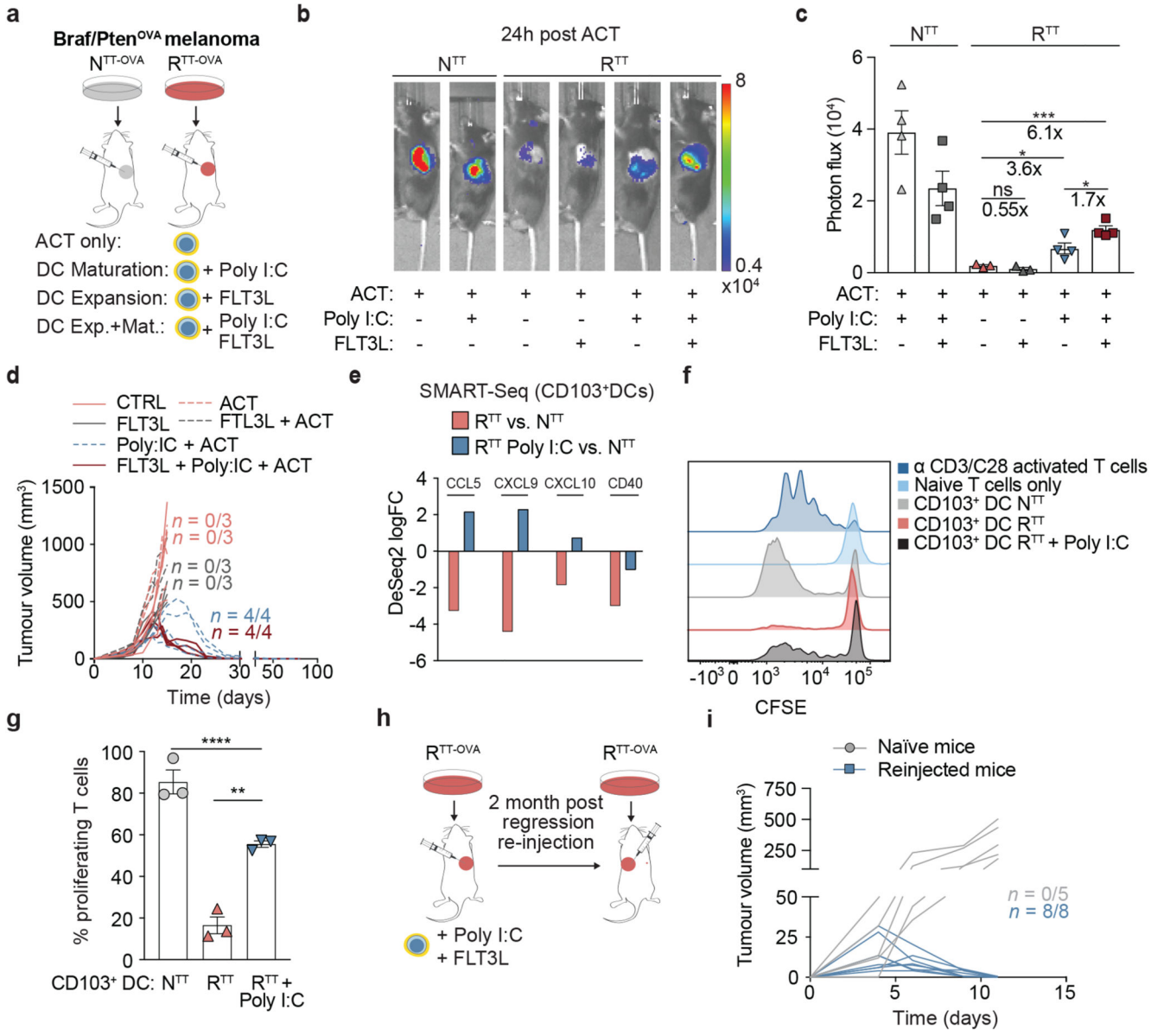


**Fig. 4. Restoration of a functional CD103$^+$ DC compartment restores immunotherapy response.**

**a,** Scheme outlining experiments to assess impact of DC maturation (intratumoural Poly I:C) and DC expansion (FLT3L overexpression from tumour cells) on ACT using effector T cells. **b, c** Tumour infiltration of OT-1$^{Luc}$ T cells in N$^{TT}$ and R$^{TT}$ Braf/Pten$^{OVA}$ melanoma measured by BLI 24 h post ACT (**b**) representative image and (**c**) quantified 24h post ACT ($n$ = 4, 4, 3, 3, 4, 4 mice from left to right). Experiment performed twice; representative example shown. $P$-value: *** 0.0004, * 0.0376, * 0.0351. **d,** Spiderplot indicating response to ACT ± Poly I:C ± FLT3L in R$^{TT}$ Braf/Pten$^{OVA}$ tumours. (R$^{TT}$ CTRL, R$^{TT}$ CTRL + FLT3L, R$^{TT}$ + ACT, R$^{TT}$ FLT3L + ACT, $n$ = 3; R$^{TT}$ + ACT + Poly I:C, R$^{TT}$ FLT3L + ACT+ Poly I:C, $n$ = 4 mice). Experiment performed twice; representative example shown. **e,** Gene expression changes in CD103$^+$ DCs sorted from Braf/Pten$^{OVA}$ N$^{TT}$, R$^{TT}$ or R$^{TT}$ tumours 24h post Poly I:C injection, assessed by Smart-seq and normalized to N$^{TT}$ (N$^{TT}$,

$R^{TT}$ + Poly I:C, $n = 4$; $R^{TT}$, $n = 5$ sorted tumours; in technical triplicates). **f,** Representative histogram illustrating CFSE signal in T cells co-cultured with $CD103^+$ DCs isolated from $N^{TT}$, $R^{TT}$ and $R^{TT}$ Braf/$Pten^{OVA}$ melanoma treated with Poly I:C. **g,** Quantification of T cell proliferation based on CFSE dilution in DC co-culture assays displayed in Fig. 4f ($n$ = 3 tumours per condition). Experiment performed once. *P*-value: **** 5E-5, ** 0.0013. **h,** Scheme illustrating experiments to address immunological memory in mice that were bearing $R^{TT}$ tumours and had complete regression in response to Poly I:C + FLT3L + ACT. **i,** Tumour growth curve in mice that previously had complete response to ACT, Poly I:C and FLT3L reinjected with $R^{TT}$ Braf/$Pten^{OVA}$ melanoma compared to naïve mice (Naïve, $n = 5$; Reinjected, $n = 8$ mice). Experiment performed twice; representative example shown. Data in **c, g** displayed as mean ± SEM and analysed using one-way ANOVA. * $P < 0.05$, ** $P < 0.01$, *** $P < 0.001$, **** $P < 0.0001$, ns= non-significant.

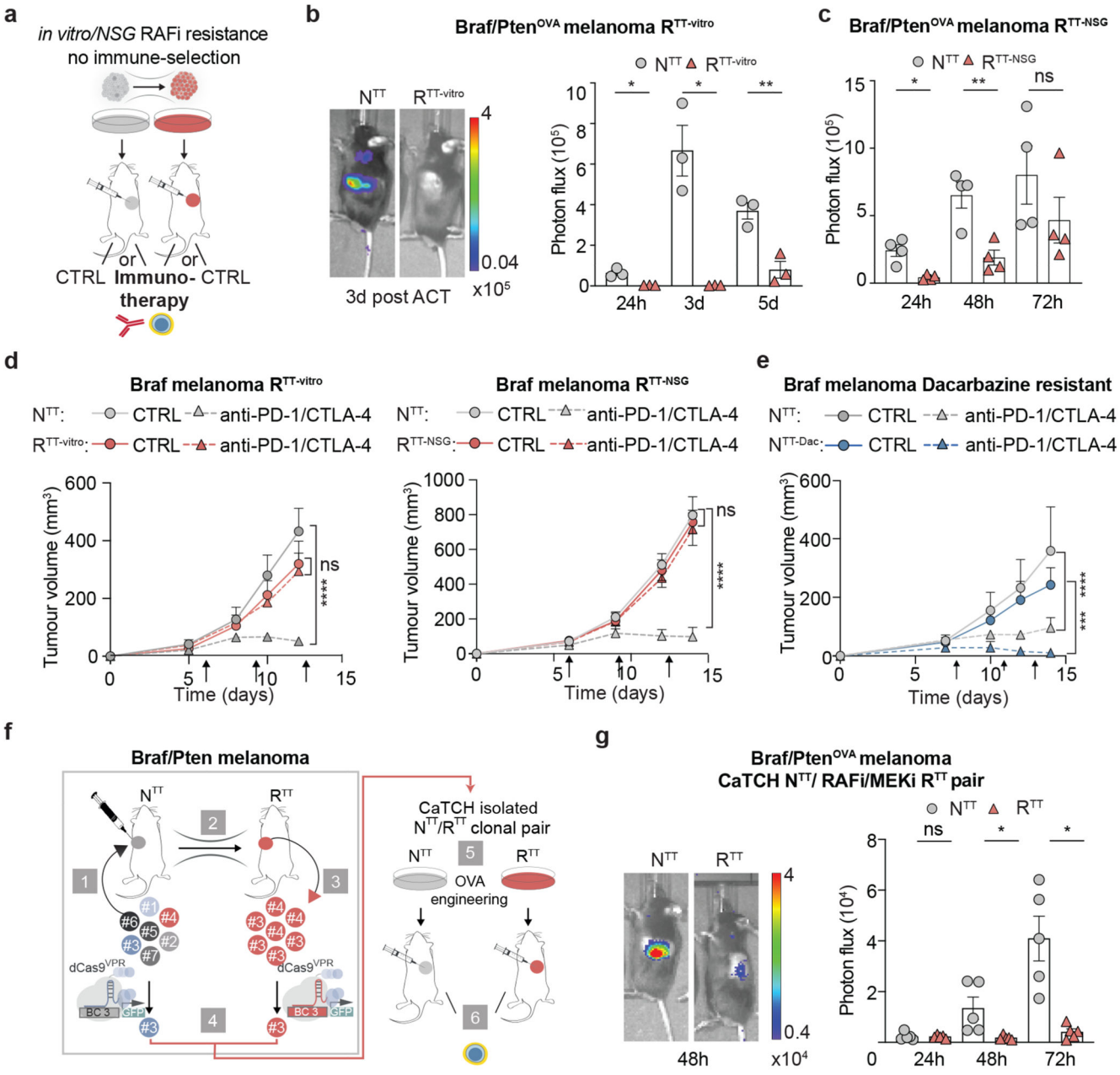


**Fig. 5. Cross-resistance is acquired during evolution of MAPKi resistance and is directly linked to a cell-intrinsic signalling program.**

**a,** Scheme outlining experiments to test ACT or anti-PD-1/CTLA-4 response in mice bearing $R^{TT\text{-}vitro}$ tumours, of cell lines made resistant *in vitro*. **b,** Tumour infiltration of OT-$1^{Luc}$ T cells into $R^{TT\text{-}vitro}$ Braf/$Pten^{OVA}$ tumours, measured by BLI at indicated days ($N^{TT}$, $n = 3$; $R^{TT\text{-}vitro}$ $n = 3$ mice). Experiment performed twice; representative example shown. *P*-value: * 0.0382, * 0.0340, ** 0.0074. **c,** Tumour infiltration of OT-$1^{Luc}$ T cells into $R^{TT\text{-}NSG}$ Braf/$Pten^{OVA}$ tumours, measured by BLI at indicated days ($N^{TT}$, $R^{TT\text{-}NSG}$, $n = 4$ mice). Experiment performed twice; representative example shown. *P*-value: * 0.0168, ** 0.0058, ns 0.2687. **d,** Treatment response to anti-PD-1/CTLA-4 in (**d**) $N^{TT}$ $R^{TT\text{-}NSG}$ (left)

and (**e**) $R^{TT\text{-}vitro}$ (right) Braf melanoma; arrows indicating therapy administration ($N^{TT}$ and $R^{TT}$ CTRL, $n = 6$; $N^{TT}$ or $R^{TT}$ IT, $n = 8$). Experiment performed 3 times; representative example shown. P-value: **** 4.8E-11, **** 7.3E-14. **e,** Treatment response to anti-PD-1/CTLA-4 in $N^{TT}$ and $N^{TT\text{-}Dacarbazine}$ Braf melanoma, arrows indicate therapy administration. ($N^{TT}$, $N^{TT\text{-}Dac}$ CTRL, $n = 6$ tumours; $N^{TT}$, $N^{TT\text{-}Dac}$ anti PD-1/CTLA-4, $n = 10$ tumours). Experiment performed once. *P*-value: **** 7.5E-5, *** 0.0008. **f,** Scheme illustrating the use of the lineage tracing system CaTCH employing a barcode guided inducible GFP reporter to isolate the treatment naïve ($N^{TT}$) founding clone of a targeted therapy resistant ($R^{TT}$) clone. Experimental steps: 1) Injection of barcoded $N^{TT}$ cell line into mice. 2) Resistance generation using RAFi/MEKi. 3) Isolation of $R^{TT}$ cell line. 4) Next-generation sequencing of barcodes in $R^{TT}$ cell line and isolation of matching $N^{TT}$ and $R^{TT}$ clones. 5) OVA engineering. 6) ACT experiment. **g,** Infiltration of OT-$1^{Luc}$ T cells into matched CaTCH isolated $N^{TT}$ and $R^{TT}$ Braf/$Pten^{OVA}$ tumours (all groups, $n = 5$ mice). Experiment performed twice; representative example shown. *P*-value: ns 0.9367, * 0.0298, * 0.0133. Data in **b, c, d, e, g** displayed as mean ± SEM. Data analysis **b, c, g** two-tailed unpaired t-test with Welch correction for unequal variance or Mann-Whitney U test if not normal distributed and **d, e** two-way ANOVA. * $P < 0.05$, ** $P < 0.01$, *** $P < 0.001$, **** $P < 0.0001$, ns = non-significant.

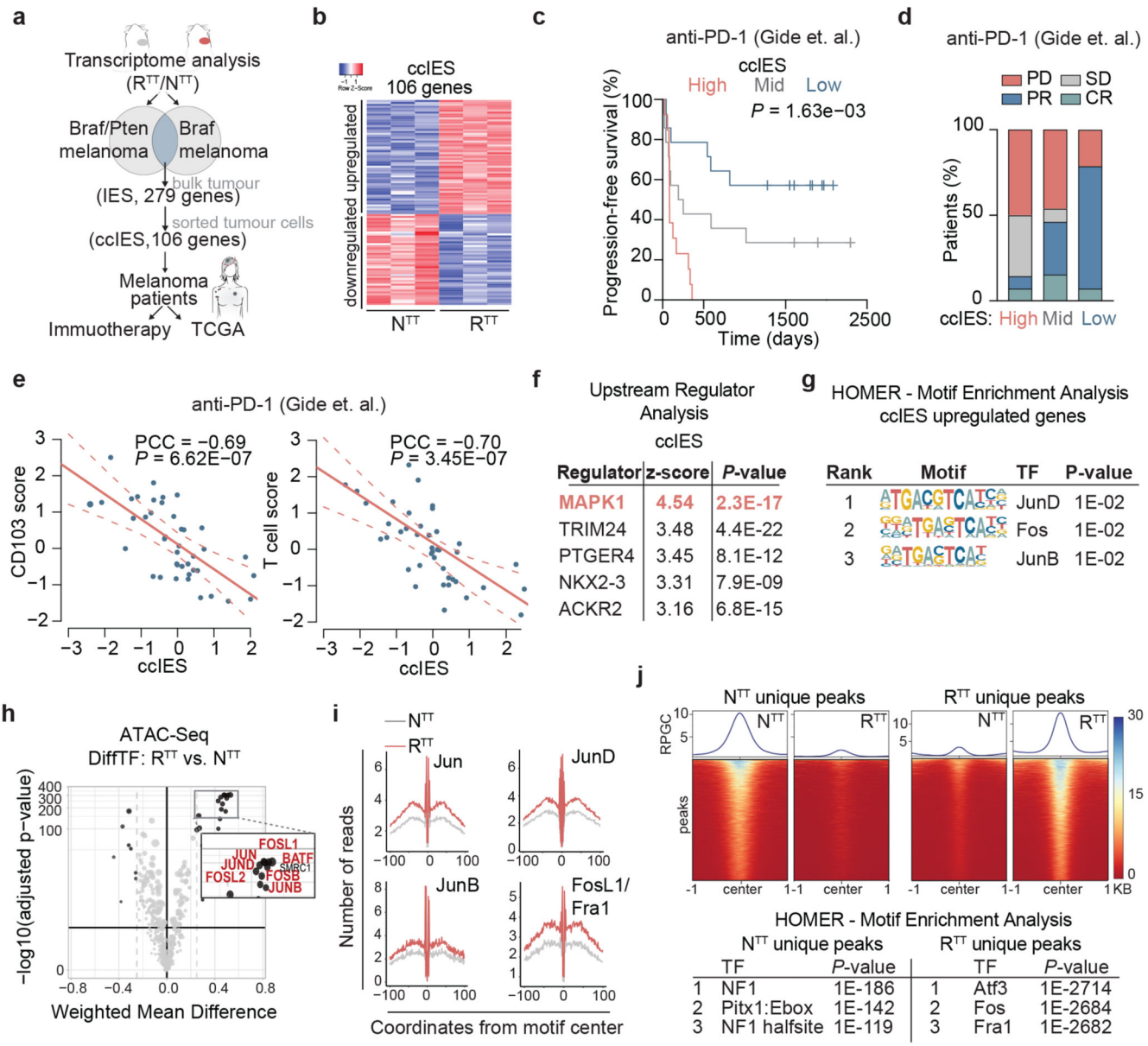


**Fig. 6. The $R^{TT}$ signalling program is predictive for immunotherapy response in patients and controlled by MAPK signalling.**

**a,** Scheme outlining the generation of the cancer cell-intrinsic immune evasion signature (ccIES, 106 genes, Supplementary Table S7) by overlapping bulk-transcriptomic data from both melanoma models (Immune evasion signature, 279 genes Supplementary Table S6) with genes deregulated in sorted Braf/Pten tumour cells. **b,** Expression of genes comprising the ccIES in $N^{TT}$ and $R^{TT}$ cancer cells sorted from Braf/$Pten^{OVA}$ tumours derived from Rag2-/-mice ($R^{TT}$ tumours in this experiment were continuously exposed to 10 mg/kg RAFi). ($n$ = 3 mice). **c,** Progression-free survival of patients receiving anti-PD-1 monotherapy ($n$ = 41 patients) stratified based on ccIES expression. **d,** Clinical response in patients receiving anti-PD-1 ($n$ = 41 patients) stratified based on ccIES expression. **e,** Correlation of ccIES with CD103 score and T cell score (Supplementary Table S8, S9) in




Europe PMC Funders Author Manuscripts

Europe PMC Funders Author Manuscripts

patients receiving anti-PD-1 ($n$ = 41 patients). **f,** Upstream regulator analysis (Ingenuity) on ccIES-genes, sorted based on z-score. **g,** HOMER motif enrichment analysis of upregulated ccIES genes, comparing $R^{TT}$ vs. $N^{TT}$. **h,** Volcano plot of differential TF activity (weighted mean difference) in ATAC-Seq data comparing $R^{TT}$ vs. $N^{TT}$ Braf/Pten$^{OVA}$ melanoma cells sorted from tumours (n= 3 tumours per condition). TFs with a TF activity >= abs (0.25) are highlighted in black. Corresponding significance is computed using the analytical approach and adjusted for multiple testing by Benjamini-Hochberg procedure (y axis). **i,** Line plots highlighting ATAC-Seq profile for indicated TF motifs in $N^{TT}$ and $R^{TT}$ Braf/Pten$^{OVA}$ cell lines. **j,** Top: Heatmap of normalized (reads per genomic content; RPGC) gene accessibility tracks (ATAC-seq). Depicted are accessibility profiles for peaks uniquely identified in $N^{TT}$ and $R^{TT}$ cell lines. Profile plots and heatmaps represent accessibility around unique peak centre (± 1KB). Heatmaps sorted by descending accessibility. Bottom: HOMER Motif enrichment analysis of peaks uniquely identified in $N^{TT}$ and $R^{TT}$ cell lines. Top 3 predicted motifs for each condition displayed. *P*-value in **c** derived from a Cox proportional hazards model using gene score as a continuous variable and analysis in **e** two-sided Pearson Correlation.

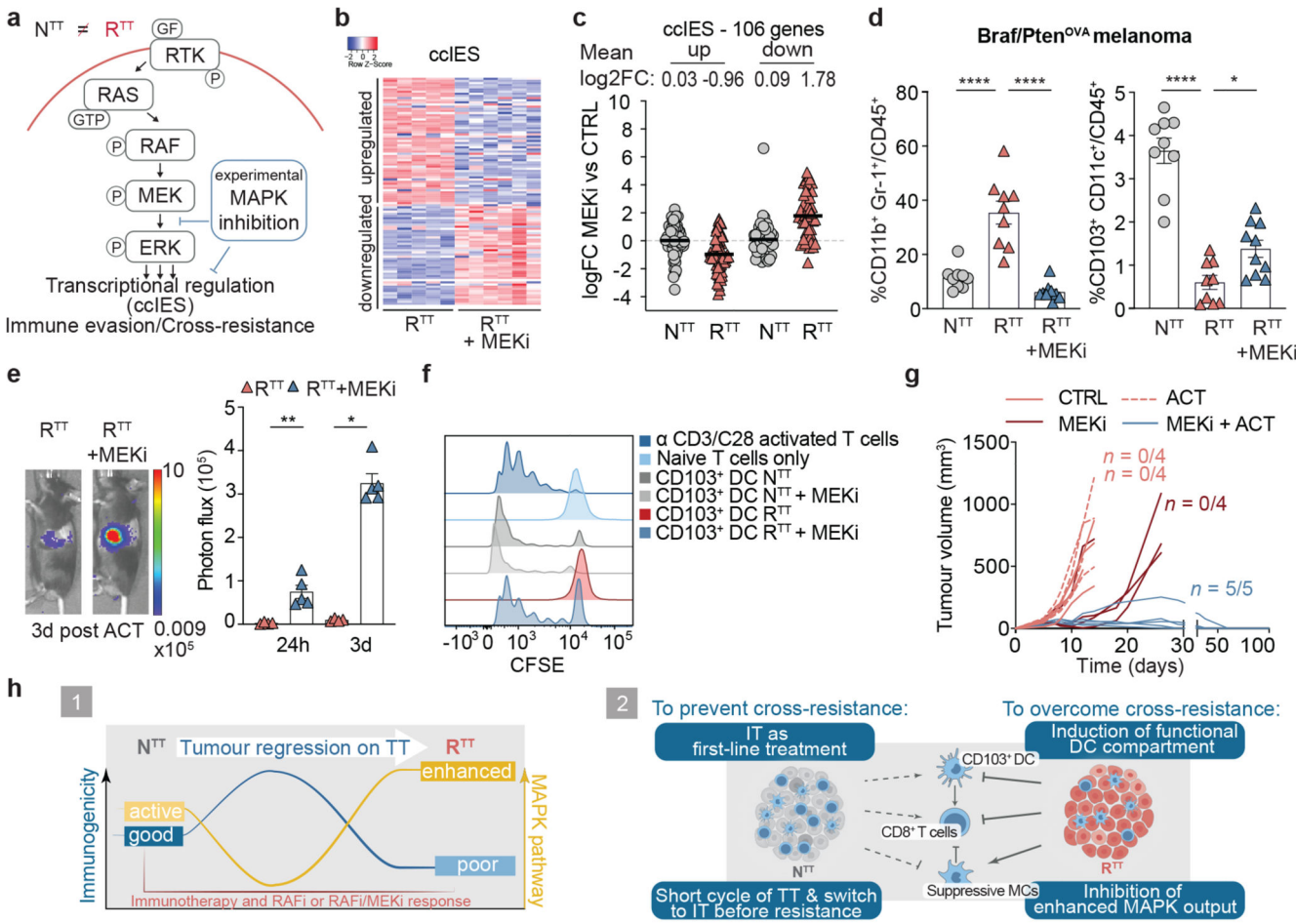


**Fig. 7. Inhibition of the re-activated MAPK pathway restores sensitivity to immunotherapy in $R^{TT}$ tumours.**

**a,** Scheme illustrating the rationale and experiment to inhibit MAPK signalling in $R^{TT}$ cells and profile the contribution of MAPK signalling to cross-resistance. **b,** Gene expression changes in ccIES-genes in response to 72h of MEKi in $R^{TT}$ Braf/Pten$^{OVA}$ melanoma cells sorted from Rag2-/-mice ($R^{TT}$, $n = 5$; $R^{TT}$+ MEKi $n = 6$ tumours). **c,** Gene expression changes analysed via SMART-Seq in ccIES genes (divided into up and downregulated genes) in $N^{TT}$ and $R^{TT}$ Braf/Pten$^{OVA}$ melanoma cells sorted from tumours after 72h of MEKi treatment ($n = 3$ tumours per condition, in technical triplicates). Black line highlights Mean. **d,** Suppressive myeloid cells and CD103$^+$ DC levels in $N^{TT}$ and $R^{TT}$ Braf/Pten$^{OVA}$ tumours 3 days post MEK inhibition ($N^{TT}$, $R^{TT}$ $n = 9$ tumours; $R^{TT}$+ MEKi, $n = 10$ tumours). Experiment performed twice; data represents pool of both experiments. *P*-value: CD11b$^+$GR-1$^+$ **** 2.5E-6, 5.2E-8; CD103$^+$CD11c$^+$ **** 2.3E-9, * 0.048. **e,** Tumour infiltration of OT-1$^{Luc}$ T cells in $R^{TT}$ Braf/Pten$^{OVA}$ melanoma, measured by BLI at indicated days post ACT, MEKi started 24h before ACT ($R^{TT}$, $n = 4$; $R^{TT}$+ MEKi, $n = 5$ tumours). Experiment performed 3 times; representative example shown. *P*-value: ** 0.0087, * 0.0159. **f,** Co-culture of CD103$^+$ DCs isolated from $N^{TT}$, $R^{TT}$ and $R^{TT}$ Braf/Pten$^{OVA}$ melanoma treated with MEKi (0.5mg/kg for 3 doses) with CFSE labelled naïve OT-1 T cells displayed as representative histogram of CFSE signal in T cells. **g,** Spider plot indicating tumour




Europe PMC Funders Author Manuscripts

volume in $R^{TT}$ Braf/$Pten^{OVA}$ tumour bearing mice treated with indicated therapies (all groups $n = 4$; except MEKi + ACT, $n = 5$ mice). Experiment performed twice; representative example shown. **h,** Summary scheme highlighting the core findings. Data in **d, e** displayed as mean ± SEM. Data analysis **d** one-way ANOVA **e** two-tailed unpaired t-test with Welch correction for unequal variance or Mann-Whitney U test if not normal distributed. * $P < 0.05$, ** $P < 0.01$, **** $P < 0.0001$, ns = non-significant.



Europe PMC Funders Author Manuscripts